Arteriosclerosis, Thrombosis, and Vascular Biology

BASIC SCIENCES

Inhibition of LXR Signaling in Human Foam Cells Impairs Macrophage-to-Endothelial Cell Cross Talk and Promotes Endothelial Cell Inflammation

Damien Leleu, Thomas Pilot, Léa Mangin, Kevin Van Dongen, Lil Proukhnitzky, Damien Denimal, Maxime Samson, Aline Laubriet, Eric Steinmetz, Mickael Rialland, Léa Pierre, Emma Groetz, Jean-Paul Pais de Barros, Thomas Gautier, Charles Thomas, David Masson

BACKGROUND: During atherogenesis, macrophages turn into foam cells by engulfing lipids present within the atheroma plaques. The shift of foam cells toward proinflammatory or anti-inflammatory phenotypes, a critical step in disease progression, is still poorly understood. LXRs (liver X receptors) play a pivotal role in the macrophage response to lipid, promoting the expression of key genes of cholesterol efflux, mitigating intracellular cholesterol accumulation. LXRs also exert balanced actions on inflammation in human macrophages, displaying both proinflammatory and anti-inflammatory effects.

METHODS: Our study explored the role of LXRs in the functional response of human macrophage to lipid-rich plaque environment. We used primary human macrophages treated with atheroma plaque extracts and assessed the impact of pharmacological LXR inhibition by GSK2033 on cholesterol homeostasis and inflammatory response. Ultimately, we evaluated macrophage and endothelial cell cross talk by assessing the impact of macrophage-conditioned supernatants on the human endothelial cell.

RESULTS: LXR inhibition by GSK2033 resulted in increased levels of cholesterol and oxysterols in human macrophages, alongside notable changes in the cholesterol ester profile. This was accompanied by heightened secretion of proinflammatory cytokines such as IL (interleukin)-6 and TNFα (tumor necrosis factor-α), despite a transcriptional repression of IL-1β. Conditioned media from GSK2033-treated macrophages more effectively activated ICAM-1 (intercellular adhesion molecule-1) and CCL2 (C-C motif ligand 2) expression in endothelial cells.

CONCLUSIONS: Our findings illustrate the intricate relationship between LXR function, cholesterol metabolism, and inflammation in human macrophages. While LXR is required for the proper handling of plaque lipids by macrophages, the differential regulation of IL-1β versus IL-6/TNFα secretion by LXRs could be challenging for potential pharmacological interventions.

GRAPHIC ABSTRACT: A graphic abstract is available for this article.

Key Words: atherosclerosis ■ endothelial cells ■ homeostasis ■ liver X receptors ■ macrophages

Atherosclerosis, a chronic inflammatory disease of the arterial wall, stands as a leading cause of morbidity and mortality worldwide.[1] Central to its pathogenesis is the intricate interplay between lipid metabolism and the immune system, particularly the pivotal role played by macrophages.[2–5] Macrophage interaction with the lipid environment of the plaque contributes to their activation. Studies using single-cell RNA-sequencing (RNA-seq) have shown that lipid-laden macrophages, resembling foam cells, initially exhibit an anti-inflammatory profile.[6–8] Trajectory analysis suggests that some of these lipid-associated macrophages develop a proinflammatory

Correspondence to: David Masson, PharmD, PhD, Université Bourgogne Europe, UMR1231, UFR des Sciences de Santé – bureau R26, 7 boulevard Jeanne d'Arc, 21000 Dijon, France, Email david.masson@chu-dijon.fr; or Damien Leleu, PharmD, PhD, Université Bourgogne Europe UMR1231, UFR des Sciences de Santé – bureau R26, 7 boulevard Jeanne d'Arc, 21000 Dijon, France, Email damien.leleu@u-bourgogne.fr
Supplemental Material is available at https://www.ahajournals.org/doi/suppl/10.1161/ATVBAHA.125.322448.
For Sources of Funding and Disclosures, see page 925.

Arterioscler Thromb Vasc Biol is available at www.ahajournals.org/journal/atvb

Nonstandard Abbreviations and Acronyms

27OHC	27-hydroxycholesterol
ABCA1	ATP binding cassette transporter A1
ABCG1	ATP binding cassette transporter G1
ATF	activating transcription factor
CCL2	C-C motif ligand 2
CE	cholesteryl ester
CREB	cAMP response element-binding protein
CXCL8	C-X-C motif ligand 8
DAPI	4′6-diamidino-2-phenylindole
GSK	GSK2033
HIF-1α	hypoxia-inducible factor-1α
hMDM	human monocyte-derived macrophage
HUVEC	human umbilical vein endothelial cell
ICAM-1	intercellular adhesion molecule-1
IL	interleukin
IL-6R	IL-6 receptor
LXR	liver X receptor
M-CSF	macrophage colony-stimulating factor
NF-κB	nuclear factor-κB
RNA-seq	RNA sequencing
TNFα	tumor necrosis factor-α
VCAM	vascular cell adhesion molecule

Highlights

- LXR (liver X receptor) inhibition in human foam cells retains cholesterol and alters cholesteryl ester composition.
- LXR inhibition in human foam cells elevates 27-hydroxycholesterol intracellularly and enriches 25-hydroxycholesterol in the supernatant.
- LXR inhibition in human foam cells activates the NF-κB (nuclear factor-κB) pathway, induces the increase of IL (interleukin)-6 and TNFα (tumor necrosis factor-α) secretion and the decrease of IL-1β expression.
- Inhibition of LXR in human foam cells has a proinflammatory effect on endothelial cells, partly due to increased IL-6 production.

pattern.[9,10] This indicates that the interaction between lipids and myeloid cells within atherosclerotic plaques is important, with macrophages transitioning from a protective to a more damaging role during atherosclerosis progression.

The lipid environment within the atherosclerotic plaque is enriched with cholesterol, oxysterols, lysophospholipids, and oxidized phospholipids.[11–13] It influences macrophages through various sensors and receptors, both at the membrane (such as CD36 [cluster of differentiation]/TLR2 [toll-like receptor]) and intracellular levels, particularly affecting several transcriptional regulatory circuits.[14,15] These pathways enable macrophages to respond and adapt to this microenvironment, notably through cholesterol esterification and efflux pathways. The nuclear receptors LXRs (liver X receptors) are key players in the macrophages' response following lipid uptake, activated by cholesterol derivatives. LXRs regulate the transcription of genes involved in cholesterol efflux pathways (ABCA1 [ATP-binding cassette transporter A1] and ABCG1 [ATP-binding cassette transporter G1]), thereby limiting the accumulation of intracellular cholesterol.[16] LXRs also directly modulate the inflammatory response of macrophages, with anti-inflammatory effects primarily observed in mouse models through various mechanisms (inhibition of TLR pathways, sumoylation mechanisms, and direct repression of proinflammatory genes).[17–19] In human macrophages, the impact of LXRs is more dichotomous, showing both proinflammatory and anti-inflammatory effects.[20–23] Our team has demonstrated that LXRs can selectively induce the transcription of the IL (interleukin)-1β gene via an HIF1α (hypoxia-inducible factor-1α)-dependent mechanism but with no impact on other proinflammatory cytokines such as TNFα (tumor necrosis factor-α) in macrophages stimulated with the TLR2 agonist PAM3CSK4 (Pam3CysSerLys4).[20] Other groups have also observed a proinflammatory impact of LXR activation on human macrophages and monocytes.[21,22] The investigation into the effects of LXR modulation in humans holds particular relevance, especially given that inverse agonists are currently undergoing early-stage clinical trials for the treatment of metabolic dysfunction–associated liver disease.[24]

The present study aimed to assess the role of LXRs in modulating the response of human macrophages to a lipid load mimicking the plaque environment. We used our previously described model of M-CSF (macrophage colony-stimulating factor) differentiated primary human monocyte-derived macrophages (hMDMs) exposed to homogenates of human atheroma plaque extracts rich in oxidized lipids.[20]

We then evaluated the impact of LXR inhibition using different LXR antagonists, GSK2033 (GSK) and SR9238,[25–27] on cholesterol homeostasis and the inflammatory response, assessed at the transcriptional level and by measuring cytokine secretion. We show that LXR inhibition results in an increased accumulation of free cholesterol and 27-OH cholesterol and a profound remodeling of the cholesterol ester profile. While we confirm the positive impact of LXRs on IL-1β at the transcriptional level, LXR inhibition also promotes an increased secretion of proinflammatory cytokines such as IL-6 and TNFα. Finally, experiments with conditioned media show that supernatants from macrophages treated with the plaque and the LXR inhibitor have a stronger capacity to activate human endothelial cells in an IL-6–dependent manner.

MATERIALS AND METHODS

The data that support the findings of this study are available from the corresponding author upon reasonable request. Please see the Major Resources Table in the Supplemental Material.

Ethics Approval and Consent to Participate

Human peripheral blood was collected from healthy donors following informed written consent, provided by the Etablissement Français du Sang (Besançon, France) in accordance with the Declaration of Helsinki. Atherosclerotic plaque extracts originated from the MASCADI cohort (Arachidonic Acid Metabolism in Carotid Stenosis Plaque in Diabetic Patients), whose protocol was reviewed and approved by the regional ethics committee (Comité de Protection des Personnes Est, Dijon, France CPP Est III, CHRU Nancy, No. 2017-A00022-51) and recorded on https://www.clinicaltrials.gov (NCT03202823). Umbilical cords, initially destined for destruction, are recovered for research purposes after the donors have been unopposed and anonymized.

Atheroma Plaque Samples

Atherosclerotic plaque extract preparation was described previously.[20] Briefly, atheroma plaque samples were obtained from patients undergoing carotid endarterectomy at the Department of Cardiovascular Surgery at the University Hospital of Dijon. Lipid-rich cores of plaque samples were carefully dissected under aseptic conditions and were homogenized with 3 volumes of cold NaCl 150 mmol/L and briefly sonicated. Samples were then frozen and stored at −70 °C before use.

Oxidized Low-Density Lipoprotein Preparation

Native LDL was isolated from plasma from healthy donors (Etablissement Français du Sang, Besançon, France) according to their density by sequential ultracentrifugation (1.019<density<1.063 g/mL). Densities were adjusted by adding solid potassium bromide salts, and ultracentrifugation runs were performed at 4 °C in a 70Ti rotor in an Optima XPN-90 ultracentrifuge (Beckman Coulter). Isolated LDL was dialyzed against 10 mmol/L Tris-buffered saline (pH 7.4), and protein concentration was adjusted to 1.2 g/L. Oxidation of LDL was performed by adding 1 volume of 30 µmol/L $CuSO_4$ solution to 5 volumes of LDL for a 24-hour incubation at 37 °C. Oxidation was stopped by adding EDTA (200 µmol/L final concentration). Oxidized LDL was finally dialyzed against PBS (pH 7.3) and sterilized through a 0.22-µm filter.

Primary Cell Cultures

Human peripheral blood monocytes were obtained from buffy coats from male and female healthy anonymous blood donors at Etablissement Français du Sang (Besançon, France). Mononuclear cells were isolated by Pancoll gradient centrifugation, and monocyte negative selection was performed via magnetic activated cell sorting using the Pan Monocyte Isolation Kit (Miltenyi Biotec, Bergisch Gladbach, Germany; catalog No. 130-117-337) according to the manufacturer's instructions. Human monocytes were differentiated into macrophages for 6 days with 50 ng/mL of M-CSF (CSF1 [colony-stimulating factor 1]; Miltenyi Biotec; catalog No. 130-093-963) into RPMI (Roswell Park Memorial Institute) 1640 medium (GIBCO; Fisher Scientific, Strasbourg, France) supplemented with 10% fetal bovine serum in 5% CO_2 and 37 °C. On day 6, hMDMs were treated for 48 hours with 1 of the following treatments: whole atherosclerotic plaque extracts (1% v/v in cell culture medium), 10 µmol/L 27-hydroxycholesterol (27OHC; Avanti Polar Lipids; Sigma; France; catalog No. 20380-11-4), or 50 µg/mL oxidized low-density lipoprotein, with or without LXR antagonist: 1 µmol/L of GSK (Sigma-Aldrich, St. Louis, MO; catalog No. 1221277-90-2) or 10 µmol/L of SR9238 (MedChemExpress, Monmouth Junction, NJ; catalog No. HY-101442). A vehicle control, dimethylsulfoxyde (Sigma-Aldrich; catalog No. D8418), was consistently included for comparison. In some experiments, hMDMs were treated with the LXR antagonist GSK, the LXR activator GW3965 (Sigma-Aldrich; catalog No. 405911-17-3), or dimethylsulfoxyde for 48 hours, followed by activation with 50 ng/mL of lipopolysaccharide (Sigma-Aldrich; catalog No. L2137) for 4 hours. At the end of culture, supernatants and cells were collected. Supernatants were centrifuged to remove cell debris and atherosclerotic plaque extracts and frozen at −20 °C before use. Cells were either recovered in RLT buffer (Qiagen, Hilden, Germany; catalog No. 74104) for mRNA extraction, in RIPA buffer (Fisher Scientific; catalog No. 89900), phosphatase inhibitor, and protease inhibitor (Thermo Fisher Scientific; catalog No. 78440) for Western blot analysis, or detached with accutase (Invitrogen, Carlsbad, CA; catalog No. A1110501) and frozen at −20 °C as dry pellets, containing around 500 000 cells, for lipidomic analysis.

Human umbilical vein endothelial cells (HUVECs) were isolated from human umbilical cords, obtained from the obstetrics department at the University Hospital of Dijon following standard procedures after childbirth and anonymization, and cultured in supplemented EBM medium (Lonza, Basel, Switzerland; catalog No. CC-3162) at 37 °C 5% CO_2. HUVECs were treated with 50 ng/mL TNFα (Miltenyi Biotec; catalog No. 130-094-014) as a positive control or with hMDM supernatants (50% v/v in cell culture medium) with or without 40 µg/mL of the anti-IL-6R (IL-6 receptor) tocilizumab (Roche, Basel, Switzerland) or with or without blocking anti-TNFα antibody (Biolegend, San Diego, CA; catalog No. 502801) for 24 hours, at a cell density of 20 000 cells/cm², on early passages (second or third passage). HUVECs were then collected in RLT buffer (Qiagen; catalog No. 74104) for mRNA extraction or detached with trypsin for cytometric analysis.

Microscopy

To assess cholesterol membrane localization and NF-κB (nuclear factor-κB) expression, human monocytes were seeded on coverslips inside the culture well. Labeling was then performed directly in the wells after cell differentiation into macrophages and previously described treatments.

For cholesterol labeling, hMDMs were incubated with the GFP-D4 (green fluorescent protein D4) probe,[28] 200-fold diluted in PBS during 30 minutes at 37 °C 5% CO_2. Cells were then fixed in 4% (v/v) paraformaldehyde for 5 minutes at room temperature and incubated with ProLong Diamond containing DAPI (4′6-diamidino-2-phenylindole; Molecular Probes; catalog No. P36966) before reading under fluorescent microscopy and confocal microscopy.

For NF-κB labeling, hMDMs were fixed in 4% (v/v) formaldehyde diluted in PBS during 15 minutes at room temperature.

Next, cells were blocked in PBS with 5% (v/v) normal goat serum and 0.3% (v/v) Triton X-100 for 1 hour. Cells were then incubated overnight with anti-NF-κB antibody (NF-κB p65 [D14E12] XP Rabbit mAb; Cell Signaling Technology, Danvers, MA; catalog No. 8242) diluted at 1:500 in antibody dilution buffer (PBS/1% BSA/0.3% Triton X-100). After rinsing with PBS, cells were incubated in fluorochrome-conjugated secondary antibody (anti-rabbit IgG [H+L], F[ab']2 fragment, Alexa Fluor 488 conjugate; Cell Signaling Technology; catalog No. 4412) diluted in antibody dilution buffer for 2 hours at room temperature in the dark. After another rinsing with PBS, cells were incubated with DAPI before mounting and reading under fluorescent microscopy.Corrected total cell fluorescence of each cell was determined using the ImageJ software. The images, featuring the fluorescence signal of the selected markers (GFP-D4 or NF-κB in green), were processed to isolate the fluorescence of interest. Subsequently, fluorescence of each cell in the image was manually quantified. The following formula was then used to calculate corrected total cell fluorescence: corrected total cell fluorescence=integrated density−(area of selected cell×mean fluorescence of background readings).

Cytokine Quantification

Cytokine assays were performed by cytometric beads array for chemokine CXCL8 (C-X-C motif ligand 8), IL-6, IL-10, IL-1β, IL-12p70, and TNFα (Cytometric Bead Array Inflammation Kit; Becton Dickinson, Franklin Lakes, NJ; catalog No.552364) and by ELISA for IL-18-BP (binding protein; R&D Systems, Inc, a Bio-Techne Brand; catalog No. DY119). Cytometric analyses were performed on LSR FORTESSA (Becton Dickinson), and absorbance readings were performed on Varioskan Lux (Thermo Fisher Scientific, Inc, Waltham, MA; NP0322BOX).

Protein Lysate and Immunoblotting

Supernatant of cultured hMDM (5 µL) and hMDM cellular lysates prepared with RIPA buffer, phosphatase inhibitor, and protease inhibitor cocktails was quantified by Western Blot analysis. Protein samples were separated by SDS-PAGE (Thermo Fisher Scientific, Inc, Waltham, MA; NP0322BOX) and transferred to either nitrocellulose (for ApoE and IL-1β; Bio-Rad, Hercules, CA; catalog No. 1704158) or PVDF membranes (NF-κB and phospho-NF-κB; Bio-Rad, Hercules, CA; catalog No. 1704156). After blocking membranes for 1 hour with 5% BSA in TBS-Tween 0.1%, primary antibodies targeting ApoE (IgG goat polyclonal; Santa Cruz Biotechnology, Dallas, TX; catalog No. sc-6384), IL-1β (IgG goat polyclonal; R&D Systems, Inc, a Bio-Techne Brand; catalog No. AF201SP), NF-κB (IgG rabbit polyclonal; Santa Cruz Biotechnology, Dallas, TX; catalog No. sc-109), and phospho-NF-κB (rabbit monoclonal antibody; Cell Signaling Technology; catalog No. 3033) were incubated overnight at 4 °C. Membranes were washed and then incubated with polyclonal rabbit anti-goat immunoglobulins (Dako; catalog No. P0449) or with polyclonal goat anti-rabbit immunoglobulins (Dako; catalog No. P0448) for 1 hour at room temperature. After further washes, chemiluminescence detection was performed using a luminol reagent Pierce ECL Western Blotting Substrate (Thermo Fisher Scientific, Inc, Waltham, MA; catalog No. 32106). Protein normalization was performed by targeting β-actin with HRP (horseradish peroxidase) anti-β actin antibody (Abcam, Cambridge, United Kingdom; catalog No. ab49900) for hMDM cellular lysates and with Ponceau S solution (Sigma-Aldrich; catalog No. P7170) for supernatant.

RT-qPCR Analysis

Total RNA was extracted using RNeasy Mini Kit (Qiagen; catalog No. 74104) according to the manufacturer's instructions. One hundred nanograms of total RNA was reverse transcribed using high-capacity cDNA reverse transcriptase (catalog No. 28025013), random primers (catalog No. 48190011), and RNaseOUT inhibitor (Invitrogen; catalog No. 10777019). cDNA obtained was quantified by real-time polymerase chain reaction using SYBR Green Rt-PCR (quantitative reverse transcription polymerase chain reaction) Kit (Invitrogen; catalog No. 4385612) and a StepOne Plus Real-Time PCR System (Applied Biosystems, CA). The ΔΔCt method was used to determine the relative mRNA levels of each gene, and Ct was normalized using 36B4 mRNA levels. Primer sequences are available on request.

Cytometric Analysis

HUVECs were first labeled with 0.02 µL BD Horizon Fixable Viability Stain 510 (Becton Dickinson; catalog No. 564406) and 20 µL FcR blocking reagent (fragment crystallizable receptor; Miltenyi Biotec; catalog No. 130-059-901) in 100 µL of cell suspension. After centrifugation, HUVECs were labeled with 0.5 µL of PE (phycoerythrin) mouse anti-human CD54 (Becton Dickinson; catalog No. 555511) and 2 µL of APC (allophycocyanin) mouse anti-human CD106 (Biolegend, San Diego, CA; catalog No. 305810) in 100 µL of cell suspension. Cytometric analysis was performed on an LSR II flow cytometer (Becton Dickinson).

Lipidomic Analysis

Lipid internal standards (17:0-cholesteryl ester [CE], 25-OH-cholesterol-d6, 27-OH-cholesterol-d6, 7α-OH-cholesterol-d7, 7β-OH-cholesterol-d7, 7-keto-OH-cholesterol-d7, and cholesterol-d7) were obtained from Avanti Polar Lipids (Croda International Plc, Alabaster, AL; catalog Nos. 700186, 700053, 700059, 700043, 700044, 700046, and 700172, respectively). LC-MS/MS (liquid chromatography with tandem mass spectrometry) quality grade solvents were purchased from Fischer Scientific. Other chemicals of the highest grade available were purchased from Sigma-Aldrich.

Macrophage dry pellets were resuspended in 200 µL of PBS. This cell suspension or 200 µL of macrophage supernatant was spiked with 10 µL of a mixture of internal standards (µg/sample: 0.5 [17:0 CE], 1 [cholesterol-d7], 0.3 [25-OH-cholesterol-d6], 0.3 [27-OH-cholesterol-d6], 0.2 [7α-OH-cholesterol-d7], 0.2 [7β-OH-cholesterol-d7], and 0.4 [7-keto-OH-cholesterol-d7]). Total lipids were further extracted by the Folch method. Organic phase was collected and dried under vaccum. Lipids were finally dissolved with 100 µL of chloroform/methanol/water 60/30/4.5 (v/v) before LC-MS/MS analysis. CEs (4 µL) were separated on a ZORBAX Eclipse Plus C8 column at a flow rate of 0.25 mL/min at 55 °C with a linear gradient of mobile phases A (methanol/water [90/10, v/v]) and B (isopropanol/methanol [90/10, v/v], both containing 10 mmol/L acetate ammonium and 1 mmol/L acetic acid as follows: 25% B for 1 minute, up to 70% B in 13 minutes,

and up to 100% in 0.1 minute and maintained at 100% for 1 minute). After each injection, the column was equilibrated 25% B for 5 minutes. Acquisition was performed on a 6490 triple quadrupole mass spectrometer (Agilent Technologies) in positive selected reaction monitoring ion. Transitions from ammonium adduct $[CE+NH_4]^+$ to cholesteryl backbone (m/z 369.3) were used for quantitation.

Each CE species was semiquantitated by calculating its response ratio regarding 17:0 CE used as internal standard. Sample used for liquid chromatography was then saponified for 45 minutes at 56 °C with 60 µL of 10 mol/L potassium hydroxide and 1.2 mL of ethanol-butylated hydroxytoluene (50 mg/L). Sterols were extracted with 5 mL of hexane and 1 mL of water. After evaporation of the organic phase, sterols were derivatized with 100 µL of a mixture of bis(trimethylsilyl) trifluoroacetamide/trimethylchlorosilane (4/1 v/v) for 1 hour at 80 °C. After evaporation of the silylating reagent, 100 µL of hexane was added. Trimethylsilylethers of sterols analysis was performed by GC-MS (gas chromatography–mass spectrometry) in a 7890A gas chromatograph coupled with a 5975C Mass Detector (Agilent Technologies). Separation was achieved on an HP-5MS 30 m×250 mm column (Agilent Technologies) using helium as carrier gas and the following gas chromatography conditions: injection at 250 °C using the pulsed split; oven temperature program: initial temperature 150 °C up to 280 °C at a rate of 15 °C/min, up to 290 °C at a rate of 1 °C/min for 2 minutes. The mass selective detector was set up as follows: electronic impact at 70 eV mode, source temperature at 230 °C. Data were acquired in single ion monitoring mode using the following quantitation ions (m/z): 131.1 for 25-OH-cholesterol, 137.1 for 25-OH-cholesterol-d6, 368.3 for cholesterol, 375.3 for cholesterol-d7, 417.4 for 27-OH-cholesterol, 423.4 for 27-OH cholesterol-d6, 456.4 for 7α-7β-cholesterol, 463.5 for 7α-7β-cholesterol-d7, 472.4 for 7-keto-cholesterol, and 479.4 for 7-keto-cholesterol-d7.

RNA-seq Analysis

RNA-seq (RNA sequencing) analysis was already described in our precedent work (GSE125126).[20] Briefly, hMDMs from 3 blood donors, each exposed to 3 distinct plaque homogenates with or without GSK, were used for RNA-seq. Total RNAs were prepared by using QIAGEN RNeasy mini kits (Qiagen; catalog No. 74104). All samples were processed simultaneously by the same operator at each step, from cell preparation, and treatment to RNA or DNA extraction. The quality of RNA was assessed using the RNA integrity number, ensuring that all samples had an RNA integrity number score above 7 before library preparation. Postsequencing quality control was conducted using FastQC to evaluate read quality, GC content, and adapter contamination. Sequencing metrics, including total reads (ranging from 40 to 71 million reads per sample), yield in megabases (12–21 Gb per sample), and Phred quality scores (mean scores between 37 and 38), were analyzed to confirm high data quality. Additionally, over 89% of bases had a Phred score of at least 30, ensuring high sequencing accuracy. mRNA purification from total RNAs and library preparation were performed with the NEBNext Ultra RNA Library Preparation Kit with poly A selection according to the manufacturer's protocols (New England Biolabs, Ipswich, MA; catalog No. E7530S). Libraries were sequenced with 2×150 bp paired-end reads on Illumina HiSeq. Sequence reads were trimmed to remove possible adaptor sequences and nucleotides with poor quality using Trimmomatic v.0.36.[29] The sequencing was performed in a single run, minimizing the risk of batch effects. The trimmed reads were mapped to the *Homo sapiens* GRCh38 reference genome using the STAR aligner v.2.5.2b. Unique gene hit counts were calculated by using feature Counts from the Subread package v.1.5.2. Only unique reads that fell within exon regions were counted. After extraction, the gene hit counts table was used for downstream differential expression analysis.

Comparison of gene expression between the groups of samples was performed using DESeq2. The Wald test was used to generate *P* values and log2 fold changes.

ATAC-Seq Analysis

ATAC-seq (assay for transposase-accessible chromatin using sequencing) analysis was performed by Active Motif company (Waterloo, Belgium) using 1×10^5 cells per sample. After 48 hours of treatment with atheroma plaque homogenates alone or in combination with the LXR antagonist GSK, cells were harvested, stored at −80 °C, and transferred to Active Motif for tagmentation, library preparation, and sequencing. Filtered reads were aligned to the GRCh38 reference genome. Open chromatin regions were identified with HOMER. Peaks were analyzed and visualized using Integrative Genomics Viewer software. The Fraction of Reads in Peaks scores were above 15% for the 2 samples, indicating high signal-to-noise ratios and acceptable data quality for analysis.

Statistical Analysis

The number of experiments was selected based on a previous study using primary human macrophages[20] with an α-risk of 5% and a power around 80%, we hypothesized a coefficient of variation of 40% and ≈2-fold changes in biological parameters following treatment with an antagonist.

The number of experiments for each panel is at least n=5 independent experiments with individual donors or individual plaque samples. RNA-seq analysis was performed with 3 independent donors; however, these exploratory transcriptomic data have been replicated by qPCR in n≥6 independent hMDM donors combined with n≥3 independent plaque homogenate donors. The same method was conducted with protein quantification. ATAC-seq analysis was exploratory only and was performed on a single donor. No statistical analysis was performed on this technique.

No statistical analysis was performed when the number of independent donors/samples was below 5. No outliers were excluded. Statistical analyses were conducted using the Prism 8 software (GraphPad), with error bars indicating the SD. In qPCR experiments, the mean ΔC(t) values from the control group (untreated samples) served as a reference in ΔΔC(t) calculations. Data are expressed as relative mRNA levels (fold mean of the control). A paired *t* test was used when the values followed a normal distribution (Shapiro-Wilk test); otherwise, a nonparametric Wilcoxon test was used. Spearman rank correlation was used to assess the correlation between 2 variables. Statistical significance was defined as $P<0.05$. An ANOVA test was performed for multigroup comparisons when all variables in the same analysis exhibited a normal distribution (Shapiro-Wilk test) with uncorrected Fisher LSD post hoc test, only if the *P* value was below the level of statistical significance ($P<0.05$). Otherwise, a Friedman test was used for nonparametric multigroup studies,

with uncorrected Dunn post hoc test conducted only if the *P* value was below the level of statistical significance ($P<0.05$).

RESULTS

LXR Inhibition Leads to Free Cholesterol Accumulation and CE Remodeling Within Macrophages

To validate our model, we analyzed the expression of prototypical LXR target genes, namely the cholesterol transporters *ABCA1* and *ABCG1*, in hMDMs exposed to plaque homogenates with or without the LXR antagonist GSK. Consistent with previous observations, incubation of hMDMs with plaque homogenates led to a marked induction of ABCA1 and ABCG1 mRNA levels (Figure 1A). This induction was completely abolished in the presence of GSK, which caused a dramatic reduction in the mRNA levels of ABCA1 and ABCG1 as compared with basal levels. We also observed a statistically significant decrease in mRNA levels of LXRα (NR1H3 [nuclear receptor subfamily 1 group H member 3]) after GSK treatment while no differences were detected for LXRβ (NR1H2 [nuclear receptor subfamily 1 group H member 2]; Figure S1).

Subsequent quantification of intracellular total cholesterol, free cholesterol, and cholesterol esters was conducted (Figure 1B). Macrophages treated with GSK-plaque combination exhibited significantly higher levels of total cholesterol and markedly elevated amount of free cholesterol compared with those treated with plaque alone. No significant differences were observed in the concentrations of cholesterol esters between the 2 groups. In parallel, we also investigated the cholesterol levels in the supernatant of macrophages treated with atheromatous plaque extracts, with and without an LXR inhibitor. As expected from our observations in the cells, LXR blockade led to a decrease in cholesterol levels in the supernatants (Figure 1C). Indeed, although we did not add exogenous cholesterol acceptors in our model, it is now recognized that macrophages can also perform autocrine cholesterol efflux. This occurs through the secretion of ApoE, which can act as an endogenous cholesterol acceptor and mediate cholesterol efflux in an LXR-dependent manner.[30] To confirm the inhibition of this pathway in our model, we quantified ApoE levels in the supernatant of hMDM conditioned with plaque extracts (Figure 1E; Figure S2). hMDMs treated with GSK displayed significantly lower ApoE levels, thus further demonstrating an inhibition of cholesterol efflux pathways.

To document the accumulation of free cholesterol at the membrane level, confocal microscopy analyses were performed using the GFP-D4 probe, which specifically targets cholesterol-enriched membrane domains. Analyses were performed on hMDMs treated with vehicle (dimethylsulfoxyde) or LXR antagonist (GSK), with atherosclerotic plaque homogenates (plaque) for 48 hours (Figure 1D). We observed that the combination of plaque and GSK resulted in a noticeable increase of GFP-D4 staining compared with the plaque-vehicle treatment.

Although GSK did not affect the total amount of cholesterol esters, we aimed to assess its impact on the relative composition of different cholesterol ester species. Cholesterol ester profiling was performed in hMDMs treated with GSK-plaque combination compared with those treated with plaque alone. Of 29 cholesterol ester species detected, 15 showed statistically significant differences between the 2 conditions. Specifically, species of saturated CEs saw an increase, with fold changes ranging from 1.4 for C16:0 CE to 3.3 for C24:0 CE. Three species of cholesteryl monounsaturated fatty acids (C20:1, C22:1, and C24:1), part of the ω9 family, also increased significantly (Figure 1F).

Thus, LXR inhibition leads to intracellular retention of cholesterol, primarily in its free form, and promotes a remodeling of the profile of cholesterol ester species toward those containing saturated or monounsaturated fatty acids.

LXR Inhibition Induces Oxysterol Accumulation and Modulate Enrichment of 25-Hydroxycholesterol in Both Intracellular and Supernatant Fraction

Subsequently, we assessed the levels of major oxysterols. Oxysterol oxidized at position 7 (7α-hydroxycholesterol and 7β-hydroxycholesterol) seems to be trending upward in macrophages treated with the GSK-plaque combination (Figure 2A and 2B). Additionally, 27OHC levels were markedly higher in the plaque-GSK group (Figure 2E) while no significant difference was observed in the levels of 7-ketocholesterol and 25-hydroxycholesterol (Figure 2C and 2D).

Furthermore, we examined the oxysterol levels in the supernatant of conditioned macrophages (Figure 2F through 2H). We found no differences in the levels of 7α-hydroxycholesterol, 7β-hydroxycholesterol, or 25-hydroxycholesterol between the supernatants of macrophages conditioned with plaque extracts, treated or not with the LXR inhibitor. Additionally, 7-ketocholesterol and 27OHC levels were undetectable. Interestingly, levels of 25-hydroxycholesterol were markedly higher in the supernatant compared with other oxysterol species, which contrasts with its lower abundance in the intracellular environment (Figure 2D and 2H). In the analysis of the enrichment of oxysterols relative to total cholesterol levels in the macrophage supernatants, we observed a statistically significant increase in 25-hydroxycholesterol, as well as a slight increase in 7α-hydroxycholesterol levels (Figure 2I).

Overall, LXR inhibition resulted in an elevation in certain oxysterols, particularly 27OHC, in macrophages treated with the plaque-GSK combination. Interestingly,

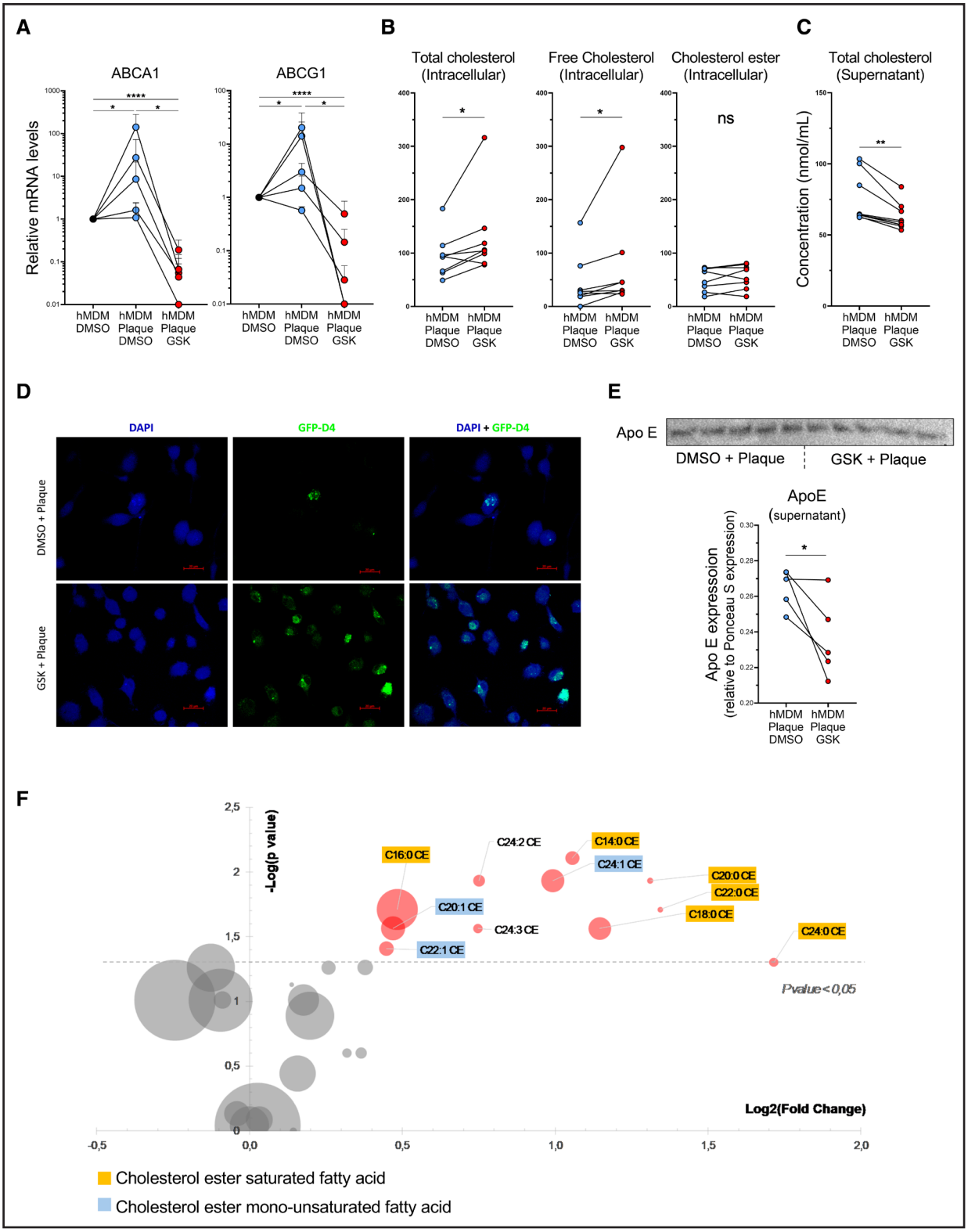

Figure 1. LXR (liver X receptor) inhibition leads to cholesterol and oxysterol accumulation and cholesterol ester remodeling in macrophages.

A, Relative mRNA levels of ABCA1 (ATP-binding cassette transporter A1) and ABCG1 (ATP-binding cassette transporter G1) in vehicle-treated human monocyte-derived macrophages (hMDMs; hMDM dimethylsulfoxyde [DMSO]), atherosclerotic plaque extract–treated hMDMs (hMDM plaque), and atherosclerotic plaque extract–treated and LXR inhibitor–treated hMDMs (hMDM plaque GSK2033 [GSK]) were assessed by RT-qPCR (quantitative reverse transcription polymerase chain reaction). Each dot represents the average response of an individual macrophage donor (nhMDM=5) treated with 3 to 6 different plaques. Bars represent mean with SD. *P<0.05, ****P<0.0001, 2-way ANOVA was used with an uncorrected Fisher LSD in post hoc analysis; normality was confirmed with the Shapiro-Wilk (*Continued*)

while no significant differences were observed in the intracellular levels of 25-hydroxycholesterol, its concentration appears significantly more abundant than other oxysterol species in the cell supernatants.

LXR Inhibition Modulates the Cytokine Response of Macrophages Exposed to Plaques

After analyzing the lipid changes induced by LXR inhibition, we turned our attention to the cytokine response, since lipid accumulation is tightly linked to the inflammatory response. We first assessed the response of macrophages exposed to plaque homogenates as compared with control macrophages (Figure 3A). RNA-seq analysis focused on the expression of genes encoding for cytokines and chemokines revealed that exposure of macrophages to plaque homogenates induced a proinflammatory profile with notable increases in several chemokines and cytokines including IL-1α, IL-1β, interleukin-1 receptor antagonist, and CXCL8. Regarding cytokine profiling in macrophage supernatant, while IL-12 and IL-1β were not detected and IL-18 levels were low, we observed that macrophages exposed to plaques secreted significantly higher levels of IL-10, IL-6, TNFα, and IL-18BP and extremely high levels of CXCL8 (Figure S3A).

To investigate the impact of LXR inhibition on cytokine expression, RNA-seq analysis was conducted on hMDMs from 3 individual donors, each treated with a different plaque homogenate, with or without GSK (Figure 3B). Consistent with previous observations, LXR inhibition significantly reduced IL-1β expression and increased IL-18BP expression. Interestingly, there was also a trend toward increased expression of CXCL8, IL-6, TNFα, and IL-10. Then, we profiled cytokines in macrophage supernatants treated with plaque homogenates along with an LXR inhibitor. Consistent with the results of RNA-seq, this cytokine profiling demonstrated an elevation in the secretion of IL-10, IL-6, TNFα, IL-18BP, and CXCL8 (Figure S3B) compared with supernatants from macrophages treated solely with plaque homogenates (Figure S3C).

To replicate these findings and to account for the interindividual variability among both donors and plaque samples, we used cells from 6 different donors, each treated with 3 to 6 independent plaque homogenates. We observed that in hMDMs treated with the combination of GSK and plaque extracts, compared with those treated with plaque alone, there was an increase in the concentration of CXCL8, IL-6, TNFα, IL-18BP, and IL-10 in cell supernatants (Figure 3C). Finally, while IL-1β was not detected in cell supernatants, the intracellular levels of pro-IL-1β were significantly lower in hMDMs treated with GSK (Figure 3D). Similar changes were also noted at mRNA levels for IL-1β, IL-6, TNFα, and IL-18BP (Figure 3E) as measured by RT-qPCR. A trend toward increased IL-10 expression was observed with GSK-plaque treatment (Figure 3E).

To confirm that the observed effects were specifically due to LXRα inhibition rather than off-target effects of GSK, we used SR9238, a distinct and selective LXR inverse agonist.[27] Similar to GSK, SR9238 significantly reduced IL-1β expression while increasing IL-18BP, TNFα, and IL-6 expression in plaque-conditioned hMDMs (Figure 3F). Analysis of supernatants further revealed elevated levels of IL-6 and TNFα (Figure 3G). These consistent findings with 2 different LXR antagonists validate the specificity of LXR inhibition in modulating inflammatory responses.

To evaluate whether the effects of LXR inhibition were consistent across various inflammatory stimuli, we tested additional models using oxidized low-density lipoprotein, 27OHC, and lipopolysaccharide. Oxidized low-density lipoprotein and 27OHC were chosen as they mimic key lipid-driven inflammatory processes observed in atherosclerosis. In hMDMs exposed to oxidized low-density lipoprotein, LXR inhibition with GSK resulted in decreased IL-1β expression and increased IL-18BP expression, as measured by RT-qPCR. IL-6 expression showed a trend toward elevation, while TNFα expression remained unchanged (Figure S4). Interestingly, 27OHC alone increased ABCA1 and IL-1β

Figure 1 Continued. normality test. **B**, Total cholesterol and cholesteryl esters in hMDMs treated with atherosclerotic plaque extracts (hMDM plaque) or atherosclerotic plaque extracts and LXR inhibitor (hMDM plaque GSK) were assessed by GC-MS and LC-MS/MS, respectively. Free cholesterol was calculated by subtracting cholesteryl esters from total cholesterol. Each dot represents the response of an individual macrophage donor (nhMDM=8) treated with a mix of 6 different plaques; *P<0.05, Wilcoxon test was performed. **C**, Total cholesterol concentration in the supernatant of hMDMs conditioned with atherosclerotic plaque extracts, treated with or without the LXR inhibitor, was assessed by GC-MS. Each dot represents the response of a macrophage donor (nhMDM=9) treated with a mix of 6 different plaques. **P<0.01, Wilcoxon test was performed. **D**, Confocal microscopy images showing staining of nuclei with DAPI (4′6-diamidino-2-phenylindole; blue) and membrane cholesterol with GFP-D4 probe (green fluorescent protein D4; green) in hMDMs following treatment with atherosclerotic plaque extracts and vehicle (plaque+DMSO) or atherosclerotic plaque extracts and LXR inhibitor (plaque+GSK). **E**, Western Blot analysis of ApoE from plaque extracts and vehicle-treated hMDMs (DMSO+plaque) and plaque extracts and LXR inhibitor–treated hMDM (GSK+plaque) supernatant form 1 hMDM donor treated with different plaque extracts. Ponceau S is used as a loading control. Graphic represents the comparison of ApoE expression relative to Ponceau S coloration between the 2 conditions. Each dot represents the response of the same hMDM donor treated with 5 different plaques. *P<0.05. Variables passed the Shapiro-Wilk normality test and were analyzed with a paired t test. **F**, Bubble plot illustrating the relative enrichment of cholesteryl ester species in atherosclerotic plaque extract–conditioned hMDMs treated with or without the LXR inhibitor. The x axis represents the log2 fold change between conditions with and without the LXR inhibitor, while the y axis represents −log10 of P values. Bubble size indicates the relative proportion of cholesteryl ester species in the LXR inhibitor condition. Red bubbles indicate statistically significant variations between the 2 conditions, as determined by the Wilcoxon test. Each dot represents the response of an individual macrophage donor (nhMDM=8) treated with a mix of 6 plaques.

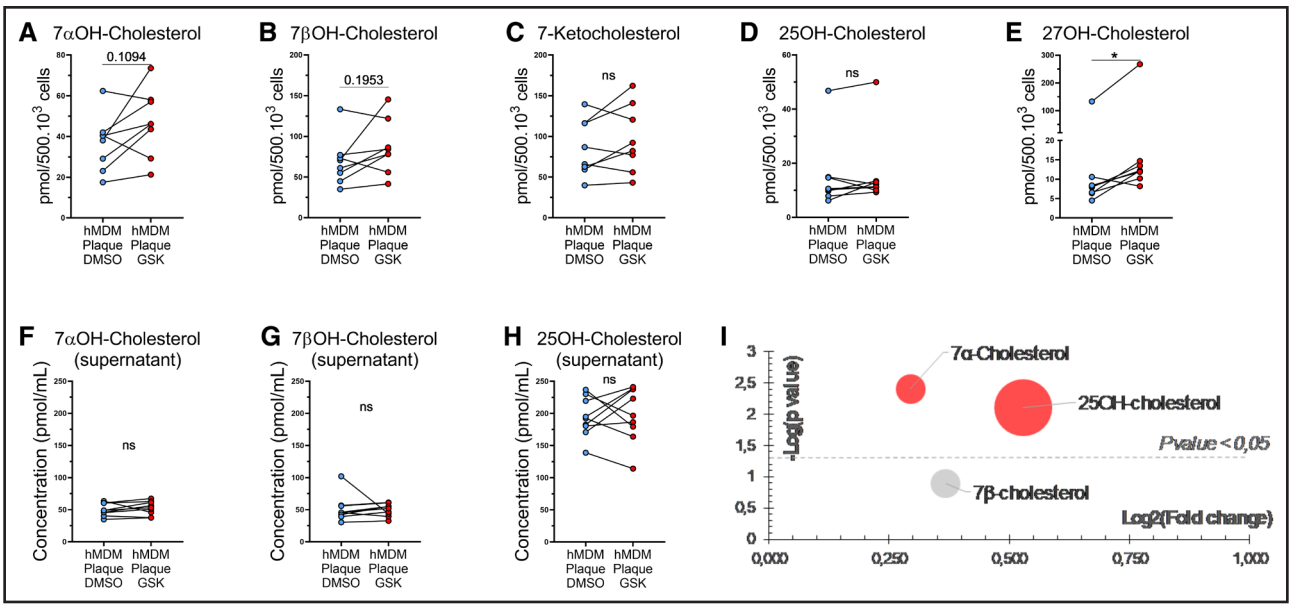

Figure 2. LXR (liver X receptor) inhibition induces oxysterol accumulation and modulates enrichment of 25-hydroxycholesterol in both intracellular and supernatant fraction.

A through **E**, Oxysterol levels (7α-OH-cholesterol [**A**], 7β-OH-cholesterol [**B**], 7-ketocholesterol [**C**], 25-OH-cholesterol [**D**], and 27-OH-cholesterol [**E**]) in human monocyte-derived macrophages (hMDMs) treated with atherosclerotic plaque extracts alone (hMDM plaque) or with the addition of an LXR inhibitor (hMDM plaque GSK2033 [GSK]) were assessed using GC-MS (gas chromatography-mass spectometry). Each dot represents the response of an individual macrophage donor (n_{hMDM}=8) treated with a mix of 6 different plaques. *P<0.05 Wilcoxon test. **F** through **H**, Concentrations of oxysterols (7α-OH-cholesterol [**G**], 7β-OH-cholesterol [**H**], and 25-OH-cholesterol [**I**]) in the supernatant of hMDMs conditioned with atherosclerotic plaque extracts, with or without LXR inhibitor treatment, were assessed using GC-MS. Each dot represents the response of an individual macrophage donor (n_{hMDM}=9) treated with a mix of 6 different plaques. *P<0.05; Wilcoxon test. **I**, Bubble plot depicting oxysterol species normalized by the total cholesterol concentration in the supernatant of hMDMs conditioned with atherosclerotic plaque extracts, with or without LXR inhibitor treatment. The *x* axis represents the log2 fold change between conditions with and without the LXR inhibitor, while the *y* axis represents −log10 of *P* values. Bubble size indicates the relative levels of oxysterol species in the LXR inhibitor condition. Red bubbles indicate statistically significant variations between the 2 conditions, as determined by the Wilcoxon test. Each dot represents the response of an individual macrophage donor (n_{hMDM}=9) treated with a mix of 6 different plaques.

expression while showing a tendency to decrease the IL-6 and IL-18BP expression (Figure S5). In all cases, LXR inhibition with GSK produced consistent effects: decreased ABCA1 and IL-1β expression and increased TNFα, IL-6, and IL-18BP expression. These findings indicate that the effects of LXR inhibition are largely similar, though not entirely identical, across plaque homogenates and other lipid-based inflammatory stimuli.

These observations were partially replicated in a model of acute inflammatory stimulation, where hMDMs were preconditioned with either GSK or GW3965 (an LXR agonist) and then exposed to lipopolysaccharide (Figure S6). While CXCL8 and TNFα secretion showed no significant differences, IL-1β and IL-18 secretion tended to decrease with GSK and, in the case of IL-1β, increase with GW3965. Conversely, IL-6 appeared to be induced by GSK and unaffected by GW3965, whereas IL-18BP secretion exhibited opposing trends to IL-18 under each treatment (Figure S6).

Effect of LXR Inhibition on Promoter Accessibility of IL-1β, IL-6, and TNFα Genes

In light of these results, we sought to identify the pathways responsible for the response to LXR inhibition. Gene set enrichment analysis of cytokines induced in macrophages incubated with plaque homogenates revealed a specific enrichment of genes regulated by RelA, among other proinflammatory transcriptional regulators, suggesting a key role for this pathway (Figure S7). Moreover, cholesterol efflux pathways are known to modulate the inflammatory response via the TLR4/Myd88/RelA (toll-like receptor 4/myeloid differentiation primary response 88/RELA) axis.[18,31]

We analyzed the chromatin accessibility of the IL-6, TNFα, IL-1β, and HIF1α promoter regions using an ATAC-seq approach in plaque-conditioned hMDMs treated with or without GSK (Figure 4; Figure S8). In macrophages treated with plaque and GSK, we observed increased chromatin accessibility in the TNFα promoter region and a slight increase in the IL-6 promoter region compared with cells treated with plaque alone. These promoter regions contained known NF-κB response elements (eg, GGATTTTCCC[32] and GGGTTTCTCC[31]) and ATF (activating transcription factor)/CREB (cAMP response element-binding protein) response elements (eg, GGACGTCA[32] and TGAGCTCA[33,34]). In contrast, little-to-no differences in chromatin accessibility were observed between GSK-treated and untreated plaque-conditioned

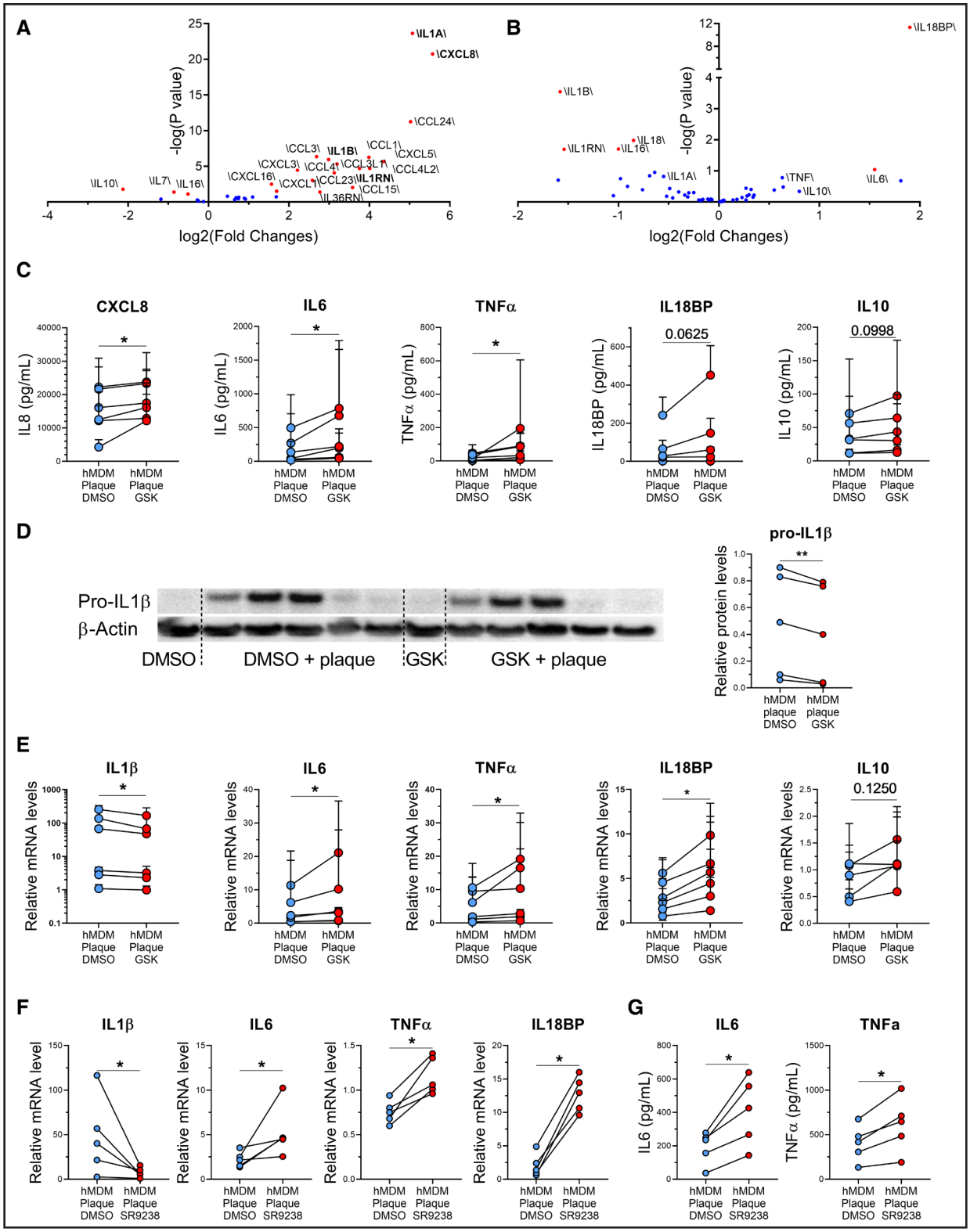

Figure 3. Cytokine response following LXR (liver X receptor) modulation.
A, Volcano plot depicting differentially expressed genes identified from RNA-sequencing data comparing untreated human monocyte-derived macrophages (hMDMs) to plaque-exposed hMDMs. Red dots represent genes with a –log(*P* value) >1. Blue dots represent genes with expression levels below this threshold. Three hMDM donors were treated with 3 different plaque extracts. A Wald test was performed to generate *P* values and log2-fold changes. **B**, Volcano plot illustrating differentially expressed genes identified from RNA-sequencing data comparing plaque-exposed hMDMs to those treated with the LXR inhibitor GSK2033 (GSK). Red dots represent genes with a –log(*P* value) >1. Blue dots represent genes with expression levels below this threshold. Three hMDM donors were treated with the same plaque extract. **C**, Analysis of cytokine production in atherosclerotic plaque extract–conditioned hMDMs treated with the LXR inhibitor (GSK) (*Continued*)

hMDMs for IL-1β and HIF1α including in regions containing hypoxia-response elements (eg, CACGT[35]) or NF-κB response elements (eg, GGATTTTCCC[36]).

Overall, these findings suggest that the RelA pathway plays a significant role in mediating the proinflammatory response to LXR inhibition, as indicated by increased chromatin accessibility in the promoter regions of IL-6 and TNFα.

LXR Inhibition Induces the NF-κB Pathway

In line with our previous observations, we assessed NF-κB activation by measuring the levels and subcellular localization of p65 using fluorescence microscopy. Exposure of macrophages to plaques increased p65 fluorescence (Figure 5A). When comparing macrophages exposed to plaques alone versus those treated with plaques and GSK, we observed a significant increase in p65 fluorescence, with a predominant nuclear localization (Figure 5A and 5B). To confirm these findings, we analyzed the expression of total and phosphorylated p65 by immunoblotting (Figure 5C and 5D). Plaque-conditioned hMDMs treated with GSK exhibited higher levels of phosphorylated p65 compared with untreated cells after both 4 and 24 hours of plaque stimulation (Figure 5C and 5D). This led to an increased phosphorylated p65/p65 ratio following LXR inhibition (Figure 5C and 5D). These results support the conclusion that LXR inhibition activates the NF-κB pathway.

LXR Inhibition in hMDMs Exposed to Plaque Homogenates Promotes Endothelial Cell Inflammation

To functionally evaluate the impact of LXR inhibition, we determined the ability of conditioned media from macrophages treated with plaque to activate human endothelial cells (Figure 6A). After treating macrophages for 48 hours with plaque±GSK, we collected the culture media to treat endothelial cells, aiming to observe changes in adhesion molecule and chemokine expression. Initial tests confirmed that unlike TNFα, neither medium culture conditioned with plaque homogenates alone (with or without GSK) nor culture media from control macrophages treated with GSK or vehicle significantly activated endothelial cells (Figure S10A). In contrast, this setup revealed that plaque extracts prompt macrophages to produce factors that activate endothelial cells, notably enhancing ICAM-1 (intercellular adhesion molecule-1) and CCL2 (C-C motif ligand 2) expression (Figure S10B and S10C). Strikingly, LXR inhibition by GSK significantly enhanced the ability of conditioned media to induce the expression of ICAM-1 by endothelial cells, both at the protein (Figure 6B) and mRNA (Figure 6D) levels, as well as VCAM (vascular cell adhesion molecule) expression at the protein level (Figure 6C) and CCL2 mRNA levels (Figure 6E).

Further investigations into the underlying mechanisms showed a direct correlation between the concentrations of IL-6 and TNFα in the conditioned media and the expression of the activation markers ICAM-1 and CCL2 by endothelial cells. Each correlation point reflects the relationship between cytokine levels in the supernatant tested on endothelial cells and the expression of endothelial cell markers. These correlations were established through flow cytometry and RT-qPCR, highlighting a strong relationship between macrophage activation and their ability to stimulate endothelial cells (Figure S9D through S9I).

To confirm the specific role of these cytokines, we tested the effects of an IL-6R inhibitor, tocilizumab, and a blocking anti-TNFα antibody on the endothelial cell response. We observed that endothelial cells treated with GSK-plaque–conditioned macrophage supernatant and tocilizumab presented lower gene expression of ICAM-1 (Figure 6F) and CCL2 (Figure 6G) as compared with endothelial cells treated only with GSK-plaque–conditioned macrophage supernatant. No significant decrease in the expression of these markers was observed with the anti-TNFα antibody (Figure S10).

In summary, LXR inhibition in plaque-conditioned macrophages exacerbates endothelial inflammation, at least partly via the IL-6 pathway.

DISCUSSION

Our work provides compelling evidence that inhibition of LXR in human macrophages exposed to human plaques has multifaceted consequences on cellular and

Figure 3 Continued. or vehicle (DMSO) by cytometric beads array (CBA) or ELISA. Each dot represents the average response of a macrophage donor (n_{hMDM}=6: CXCL8 [C-X-C motif ligand 8], IL [interleukin]-6, TNFα [tumor necrosis factor-α], and IL-10; n_{hMDM}=5: IL-18BP) treated with 3 to 6 different plaques. Bars represent mean with SD. *P<0.05; Wilcoxon test was performed. **D**, Western blot analysis of intracellular pro-IL-1β in hMDMs from 1 donor treated with different plaque extracts, with vehicle (DMSO) or with LXR inhibitor (GSK). β-actin was used as a loading control. Each dot represents the response of the same hMDM donor treated with 5 different plaques. **P<0.01; variables passed the Shapiro-Wilk normality test and were analyzed with a paired *t* test. **E**, Analysis of cytokine expression in atherosclerotic plaque extract–conditioned hMDMs treated with the LXR inhibitor (GSK) or vehicle (DMSO) by RT-qPCR (quantitative reverse transcription polymerase chain reaction). Each dot represents the average response of a macrophage donor (n_{hMDM}=6) treated with 3 to 6 different plaques; bars represent mean with SD. *P<0.05, Wilcoxon test was performed. **F**, Analysis of cytokine expression in atherosclerotic plaque extract–conditioned hMDMs from 1 donor, conditioned with 5 different plaque extracts and treated with LXR inhibitor (SR9238) or vehicle (DMSO) by RT-qPCR; bars represent mean with SD. *P<0.05, Wilcoxon test was performed. **G**, Analysis of cytokine secretion in atherosclerotic plaque extract–conditioned hMDMs from 1 donor, conditioned with 5 different plaque extracts and treated with the LXR inhibitor (SR9238) or vehicle (DMSO) by ELISA. *P<0.05, Wilcoxon test was performed. *P* value was calculated 2 tailed for all analyses using GSK and in 1 tailed for analysis using SR9238, as SR9238 was used to confirm the effect induced by GSK. CBA indicates cytometric beads array.

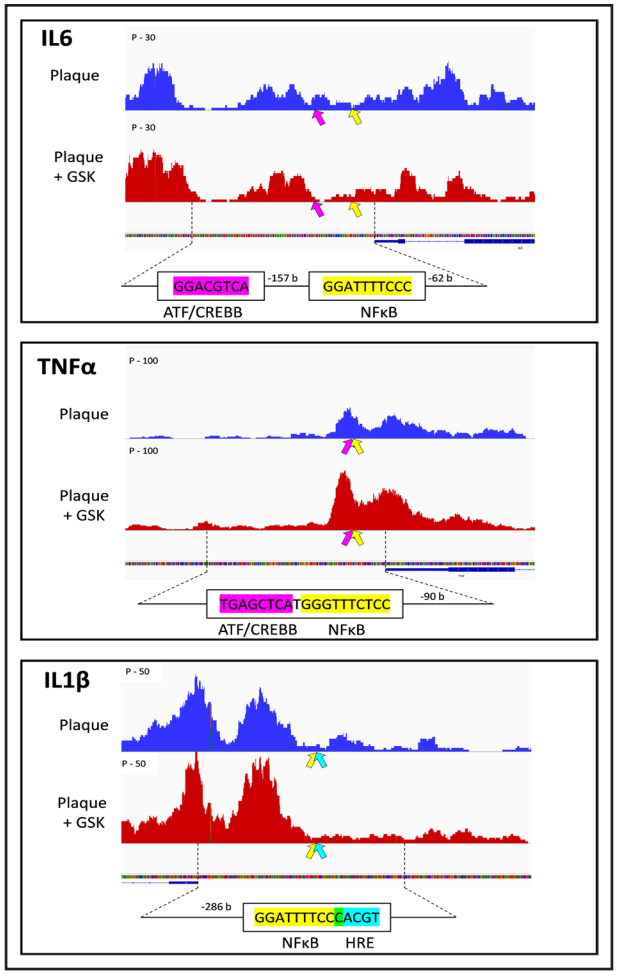

Figure 4. Effect of LXR (liver X receptor) inhibition on promoter accessibility of IL (interleukin)-1β, IL-6, and TNFα (tumor necrosis factor-α) genes.
Graphical representation of ATAC-seq (assay for transposase-accessible chromatin using sequencing) data for IL-6, TNFα, and IL-1β genes, comparing chromatin accessibility in an human monocyte-derived macrophage (hMDM) donor treated with atherosclerotic plaque extracts (blue) vs an hMDM donor treated with atherosclerotic plaque extracts and the LXR inhibitor GSK2033 (red). The dotted area represents the gene's promoter region. Highlighted sequences correspond to ATF (activating transcription factor)/CREB (cAMP response element-binding protein; pink), NF-κB (nuclear factor-κB; yellow), and hypoxia-response element (HRE; blue) response elements. n_{hMDM}=1, n_{Plaque}=1.

inflammatory responses, shedding light on the intricate interplay between cholesterol homeostasis and immune regulation.

Initial approaches of single-cell RNA-seq in atherosclerotic plaques have led to a paradigm shift, unexpectedly revealing that lipid-laden macrophages exhibited mainly an anti-inflammatory profile.[6,7] While subsequent studies have also identified populations of foamy macrophages with a proinflammatory profile,[9,10] these insights have heightened the importance of further research aimed at uncovering the underlying mechanisms that drive the transformation of these lipid-laden macrophages into proinflammatory foam cells, with the potential to open new therapeutic avenues for atherosclerosis treatment. In atheroma plaques, engulfment of lipid molecules from the plaque microenvironment (cell debris or lipoproteins) by macrophages promotes foam cell formation. Among the other pathways, the plaque milieu, rich in cholesterol and its oxidized derivatives, activates the nuclear receptor LXR, a major regulator of cholesterol homeostasis and inflammation. We have previously demonstrated that an LXR-HIF-1α regulatory pathway positively regulates IL-1β expression in human macrophages and that a pharmacological LXR antagonist effectively inhibits IL-1β expression in vitro in human foam cells.[20] However, we pointed out that the suppression of cholesterol transporters ABCA1 and ABCG1 in the presence of the LXR inhibitor may have negative consequences on cholesterol homeostasis.[20]

Indeed, we demonstrate here that LXR inhibition in macrophages exposed to a lipid microenvironment mimicking the content of human carotid plaques is accompanied by significant alterations in cholesterol homeostasis. While the accumulation of free cholesterol was expected, due to the deficit in cholesterol efflux pathways, we show that LXR inhibition, while not altering the total amount of cholesterol esters, significantly remodels their fatty acid composition, with an increase in the proportion of species containing saturated and monounsaturated fatty acids. Intracellular cholesterol is constantly subjected to opposite esterification or hydrolysis reactions that modulate cholesterol storage and transport. Notably, the hydrolysis of intracellular cholesterol esters is a crucial step for the mobilization and efflux of cholesterol from foam cells.[37] Although this area has been underexplored, it is now clear that the fatty acid chains of cholesterol esters are key determinants in regulating the hydrolysis of CE or lipid droplet homeostasis. CE hydrolases, in fact, have different affinities depending on the fatty acid chain esterifying the cholesterol.[38] Furthermore, the length of the carbon chains and the degree of unsaturation of the fatty acids can modulate the structure of the lipid droplets, as well as the oxidation of the lipid molecules within the droplet.[39–41] To the best of our knowledge, our study thus demonstrates a new role for LXR in intracellular cholesterol ester homeostasis that will need to be explored further, with a potential impact on the cholesterol availability for efflux and hence on the whole reverse cholesterol transport process.[42]

In parallel with the accumulation of free cholesterol, our study also reveals that LXR inhibition leads to elevated levels of certain oxysterols, particularly 27-OH cholesterol. Prior research has underscored the significant role of the cholesterol transporter ABCG1 in facilitating the efflux of oxysterols such as 7-ketocholesterol from macrophages, which could account for the heightened oxysterol levels observed in our model.[43] The influence of oxysterols on macrophages within the atherosclerotic milieu has been

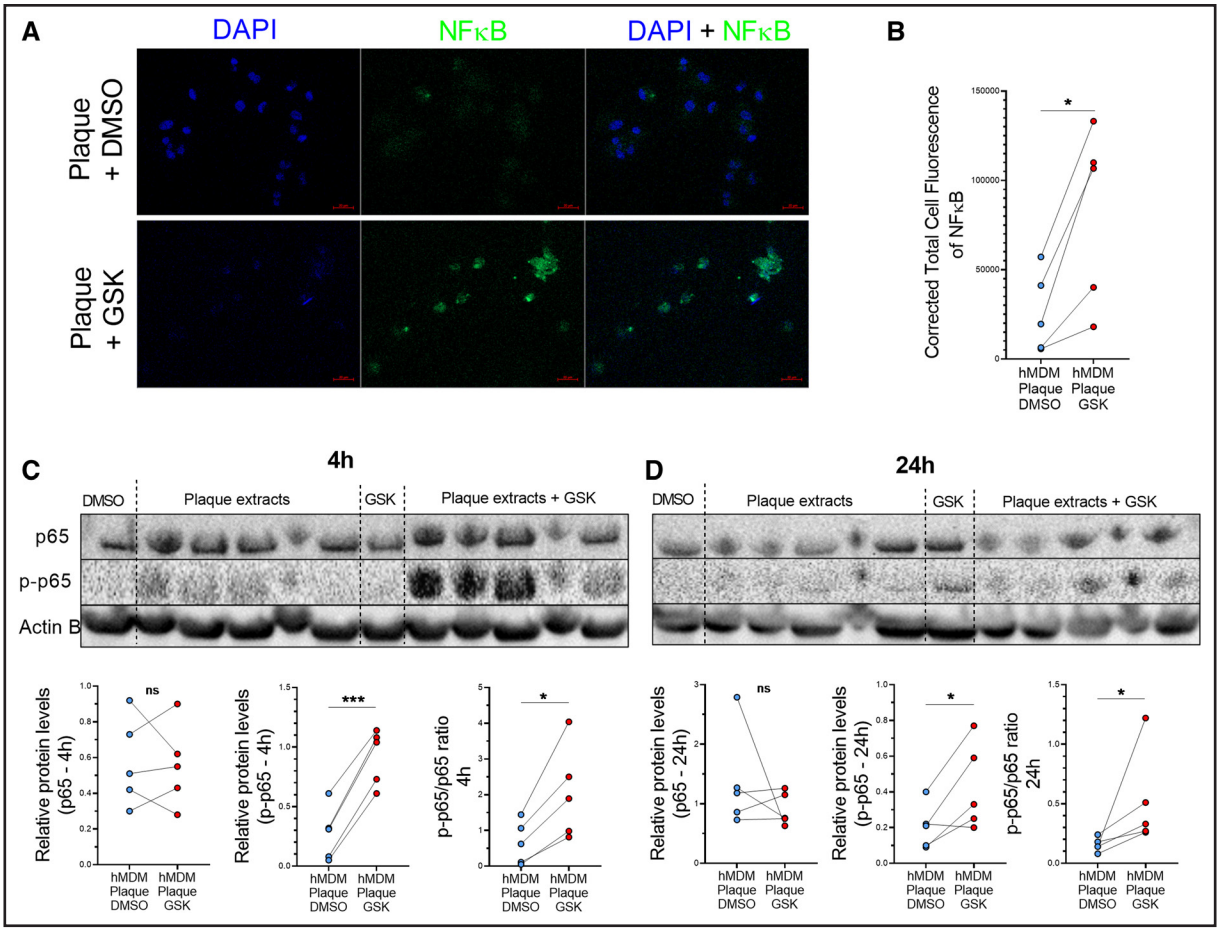

Figure 5. LXR (liver X receptor) inhibition induces the NF-κB (nuclear factor-κB) pathway.
A, Fluorescent microscopy images showing atherosclerotic plaque extract–treated and vehicle-treated human monocyte-derived macrophages (hMDMs; plaque+DMSO), and atherosclerotic plaque extract–treated and LXR inhibitor–treated hMDMs (plaque+GSK2033 [GSK]). Nuclei were stained with DAPI (4′6-diamidino-2-phenylindole; blue), and NF-κB was stained with a specific antibody (green). **B**, Cell total corrected fluorescence of NF-κB compared between hMDMs treated with atherosclerotic plaque extracts alone (plaque+DMSO) and those treated with atherosclerotic plaque extracts and LXR inhibitor (plaque+GSK) from 1 donor treated with 5 different atheroma plaques separately. *P<0.05; variables passed the Shapiro-Wilk normality test and were analyzed with a paired t test. **C**, Western blot analysis of total p65 and phosphorylated p65 forms of NF-κB from hMDMs treated with vehicle (DMSO), LXR inhibitor (GSK), plaque extracts and vehicle (plaque extracts), and both LXR inhibitor and plaque extracts (plaque extracts+GSK) during 4 hours. β-Actin was used as a loading control. Graphics represent, from **left** to **right**, total p65 relative protein levels, phosphorylated p65 relative protein, and phosphorylated p65/total p65 ratio. Each dot represents the response of the same hMDM donor treated with 5 different plaques. *P<0.05, ***P<0.001; variables passed the Shapiro-Wilk normality test and were analyzed with a paired t test. **D**, Western blot analysis of total p65 and phosphorylated p65 forms of NF-κB from hMDMs treated with vehicle (DMSO), LXR inhibitor (GSK), plaque extracts and vehicle (plaque extracts), and both LXR inhibitor and plaque extracts (plaque extracts+GSK) during 24 hours. β-Actin was used as a loading control. Graphics represent, from **left** to **right**, total p65 relative protein levels, phosphorylated p65 relative protein, and phosphorylated p65/total p65 ratio. Each dot represents the response of the same hMDM donor treated with 5 different plaques. *P<0.05; variables passed the Shapiro-Wilk normality test and were analyzed with a paired t test. p-p65 indicates phosphorylated-p65.

thoroughly investigated, highlighting their impact on macrophage phenotype modulation. These effects are mediated through both LXR-dependent and independent mechanisms, reflecting their diverse biological activities. Indeed, oxysterols play critical roles in altering cellular metabolism and exerting proinflammatory and proapoptotic effects.[44–46] The levels of 25-OH-cholesterol do not seem to vary with LXR inhibition within macrophages. Conversely, when looking at oxysterol concentrations in the macrophage supernatants, 25-OH-cholesterol was the most abundant species; moreover, its relative levels (normalized by the cholesterol content) were significantly increased by LXR inhibition. It has already been described that 25-OH-cholesterol participates in promoting atherogenesis, particularly by compromising endothelial integrity, vasodilation, as well as increasing plaque instability through enhanced inflammatory response of lipid-laden macrophages, and by inhibiting smooth muscle cell proliferation within the plaque.[47,48]

In a second step, we evaluated the secretion of cytokines by macrophages. Previous work from our team mainly focused on transcriptional regulation,[20] but this only

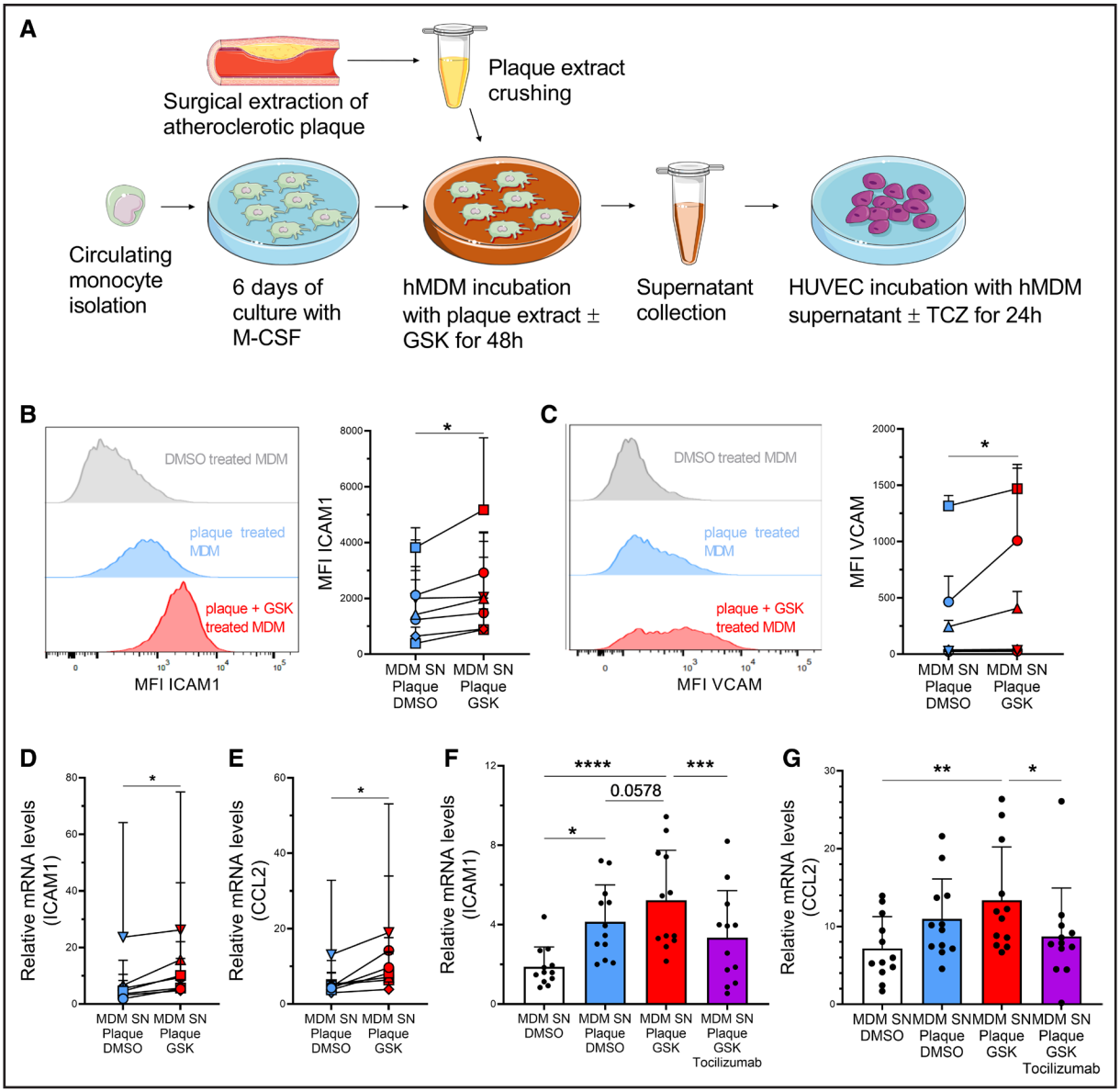

Figure 6. Supernatant from human monocyte-derived macrophages (hMDMs) conditioned with plaque homogenates and LXR (liver X receptor) antagonist induces a proinflammatory state in endothelial cells.

A, Schematic representation of the procedure used to treat endothelial cells with conditioned macrophage supernatants. **B**, **Left**, Histograms displaying ICAM-1 (intercellular adhesion molecule-1) fluorescence levels in endothelial cells cultured with supernatants from DMSO-treated hMDMs, plaque-treated MDMs, and plaque+GSK2033 (GSK)-treated MDMs. **Right**, Comparison of ICAM-1 mean fluorescence intensity (MFI) in human umbilical vein endothelial cells (HUVECs) treated with supernatants from hMDMs conditioned with various plaque extracts, either alone (blue points) or in combination with an LXR inhibitor (GSK; red points). Each point represents the average effect of supernatants from 6 different hMDMs, conditioned with 3 to 6 different plaque extracts, on HUVECs. Bars represent mean with SD. *P<0.05, Wilcoxon test was performed. **C**, **Left**, Histograms displaying VCAM (vascular cell adhesion molecule) fluorescence levels in endothelial cells cultured with supernatants from DMSO-treated hMDMs, plaque-treated MDMs, and plaque+GSK-treated MDMs. **Right**, Comparison of VCAM mean fluorescence intensity (MFI) in HUVECs treated with supernatants from hMDMs conditioned with various plaque extracts, either alone (blue points) or in combination with an LXR inhibitor (GSK; red points). Each point represents the average effect of supernatants from 6 different hMDMs, conditioned with 3 to 6 different plaque extracts, on HUVECs. Bars represent mean with SD. *P<0.05, Wilcoxon test was performed. **D** and **E**, Comparative analysis of relative mRNA levels of ICAM-1 (**D**) or CCL2 (C-C motif ligand 2; **E**) by RT-qPCR (quantitative reverse transcription polymerase chain reaction) in HUVECs treated with supernatants from hMDMs conditioned with various plaque extracts, either alone (blue points) or in combination with an LXR inhibitor (GSK; red points). Each point represents the average effect of supernatants from 7 different hMDMs, conditioned with 3 to 6 different plaque extracts, on HUVECs. Bars represent mean with SD. *P<0.05, Wilcoxon test was performed. **F** and **G**, Relative mRNA levels of targeted gene (ICAM-1 [**F**] and CCL2 [**G**]) in HUVECs treated with DMSO-treated hMDM supernatant, atherosclerotic plaque extract–treated hMDM supernatant, atherosclerotic plaque extract–treated and LXR inhibitor– treated hMDM supernatant, and atherosclerotic plaque extract–treated and LXR inhibitor–treated hMDM supernatant with tocilizumab (40 µmol/L). Each dot represents the response of supernatants from 12 different hMDMs, conditioned with a mix of 6 different plaques, on HUVECs. Bars represent mean with SD. *P<0.05, **P<0.01, ***P<0.001; Friedman test was performed with uncorrected Dunn post hoc test for multivariate analyses. M-CSF indicates macrophage colony stimulating factor; and TCZ, tocilizumab.

partially reflects cytokine secretion by cells. Analysis of a panel comprising major proinflammatory cytokines and chemokines in the supernatants of plaque-conditioned macrophages confirms that these cells exhibit a proinflammatory phenotype with significant levels of CXCL8, TNF-α, and IL-6 secreted in the medium.[49–52] CXCL8 is notably produced at higher levels by macrophages in atherosclerotic plaques, promoting inflammatory cell recruitment, angiogenesis, and neovascularization, and plays a crucial role in the development and progression of atherosclerosis, which is consistent with our data.[53,54] However, in line with our previous studies, we did not find significant levels of IL-1β in cell supernatants in the absence of inflammasome activation.[20] Therefore, while we confirm the strong dependence of IL-1β on LXR regulation at the transcriptional level, with a marked decrease in IL-1β mRNA levels in the presence of the GSK molecule, it does not affect IL-1β concentration in cell supernatants, with undetectable levels in all cases. Nevertheless, intracellular pro-IL-1β was significantly decreased with LXR inhibition, confirming our transcriptional results. In line with our previous work, we report the negative regulation of IL-18BP by LXR.[20] IL-18BP is a natural inhibitor of the proinflammatory cytokine IL-18, which belongs to the IL-1 family like IL-1β.[55] These results confirm an opposite regulation between murine and human macrophages.[56]

In our system, the observed increase in IL-18BP following LXR inhibition aligns with the decrease in IL-1β and IL-18, especially in the case of TLR activation, as these 2 cytokines require inflammasome activation for their secretion. These findings differ from those of Pourcet et al,[56] who reported increased IL-1β and IL-18 expression after silencing LXRα and LXRβ in human macrophages. This discrepancy may stem from our use of an inverse agonist, which modulates receptor activity differently from its absence. Additionally, the transfection procedure induced an inflammatory response in primary macrophages, complicating comparisons with nontransfected cells.[57] Importantly, we show a significant impact of LXR inhibition on the concentrations of proinflammatory cytokines such as TNF-α and especially IL-6, these alterations being also found at the transcriptional level. This apparent dichotomy likely arises from the distinct transcriptional regulation of these genes. IL-1β is a well-established HIF1α target, and our previous work demonstrated that LXR potentiates the HIF1α response.[20] The direct or indirect interaction between LXR and HIF1α at the IL-1β promoter could explain why IL-1β expression is suppressed upon LXR inhibition. In contrast, TNF-α and IL-6 appear to be primarily regulated by the NF-κB pathway but not by HIF1α.[58] Our data show that LXR inhibition enhances the phosphorylation of NF-κB p65, leading to increased expression of TNF-α and IL-6. We have conducted ATAC-seq analysis of the gene promoters, showing increased chromatin accessibility at IL-6 and TNF-α promoters but no changes for IL-1β or HIF1α. Taken together, our study suggests that the opposing effects of LXR could be driven by its ability to differentially modulate the HIF1α and NF-κB pathways, resulting in distinct regulatory outcomes for target genes such as *IL-1β*, *TNF-α*, and *IL-6*. Nevertheless, it remains tempting to link NF-κB activation with the accumulation of cholesterol we observed in the cellular membrane. Indeed, impaired efflux and free cholesterol accumulation have been associated with the activation of TLR pathways and a proinflammatory macrophage phenotype.[18,31] Alternatively, the trend toward the accumulation of oxysterols, such as oxidized derivatives at position 7 with a strong inflammatory potential, might also contribute to NF-κB activation. Overall, these results, coupled with recent works from our group, point toward a dual effect of LXR depending on the pathways considered, with a positive regulation of IL-1β via LXR-HIF1α.[20] Conversely, in a cholesterol/oxysterol-enriched milieu, there is a broader impact of LXR on NF-κB pathways and the IL-6 and TNF-α secretion, potentially via cholesterol efflux pathways.

Based on our observations on cytokine response, we were interested in investigating the consequences on the interaction of macrophages with other cell types within the atheroma plaque. We chose to focus on the interplay between macrophages and endothelial cells since both endothelial dysfunction and inflammation are hallmark of atherosclerosis[59,60] and macrophages play a crucial role in promoting endothelial dysfunction by communicating with endothelial cells. This interplay primarily occurs through the secretion of cytokines and chemokines.[61] Macrophages, in response to lipid accumulation, produce proinflammatory molecules that induce the expression of adhesion molecules on endothelial cells. These adhesion molecules facilitate the recruitment of other immune cells, thus perpetuating the inflammatory cycle. We showed that conditioned medium from macrophages incubated with the LXR antagonist induces an increase in the expression of CCL2, ICAM-1, and VCAM, involved in the recruitment and adhesion of monocytes. TNFα produced by macrophages has already been described as directly promoting the inflammatory state of the endothelial cell,[62,63] but the effects are more complicated concerning IL-6. Due to the low expression of IL-6R by endothelial cells, signaling via IL-6 to the endothelial cell is thought to mainly occur by trans-signaling with soluble IL-6R/IL-6 complexes interacting with GP130, a transmembrane glycoprotein that enables intracellular signal transmission.[64] In addition to IL-6, macrophages express significant levels of IL-6R and produce soluble IL-6R, reinforcing the hypothesis of this trans-signaling pathway.[64,65] Moreover, treating endothelial cells with tocilizumab, an antibody inhibiting IL-6R, reduces the effects of the conditioned medium, demonstrating the involvement of IL-6. Nevertheless, the contribution of other cytokines or mediators, notably TNFα and oxysterols, cannot be excluded. Although we did not observe any effect

with the addition of blocking the anti-TNFα antibody, it is important to note that TNFα concentration remains lower in our macrophage than IL-6 concentration, which may explain the greater contribution of this cytokine to the endothelial cell response. The impact of oxidized cholesterol derivatives on endothelial function is well described as discussed above for 25-OH-cholesterol.[47,48,66] Indeed this oxysterol can notably modulate endothelial functions, including inflammatory responses and barrier integrity.[47] Recently, an important role of 27-OH cholesterol in the macrophage-to-endothelial cell cross talk has been demonstrated.[67] The impact of these lipid mediators in our system remains to be explored. Furthermore, it is noteworthy that lipidated ApoE, secreted by macrophages, has been shown to inhibit the expression of the endothelial adhesion molecule, VCAM,[68] which could contribute to some of the effects we observed in the present study. Indeed, we observed that LXR inhibition reduced the secretion of ApoE in human macrophage supernatant and an increase of VCAM expression at the surface of endothelial cells treated with plaque extract-GSK conditioned macrophage supernatants.

In conclusion, the objective of our study was to investigate in vitro the role of the LXR response in controlling the inflammatory potential of foam cell macrophages in a model mimicking the natural environment of the atherosclerotic plaque and to evaluate its functional consequences. We demonstrate that LXR is essential for lipid homeostasis and the inflammatory response in this context. While we confirm the positive regulation of IL-1β by LXR, it does not appear to play an essential role in our model. On the contrary, alterations in cholesterol homeostasis associated with the activation of NF-κB orientate macrophages toward a more inflammatory and potentially deleterious functional phenotype, as evaluated here by the interaction with endothelial cells. These results demonstrate that pharmacological manipulation of LXR is delicate to implement due to the complex interactions of LXR with cholesterol metabolism and inflammation within human macrophages and notably the opposite regulation between IL-1β and IL-6/TNFα.

ARTICLE INFORMATION

Received January 29, 2025; accepted March 24, 2025.

Affiliations

Center for Translational and Molecular Medecine (CTM), INSERM, UMR1231, Université Bourgogne Europe, Dijon, France (D.L., T.P., L.M., K.V.D., J.-P.P.B., T.G., C.T., D.M.). LipSTIC LabEx, Université Bourgogne-Franche compté, Dijon, France (D.L., T.P., L.M., K.V.D., J.-P.P.B., T.G., C.T., D.M.). DiviOmics Platform, UMS58 BioSanD, INSERM, Université de Bourgogne Europe, Dijon, France (J.-P.P.B.). Department of Clinical Chemistry (D.L., D.D., D.M.), Department of Internal Medicine (M.S.), and Department of Cardiovascular Surgery (A.L., E.S.), CHU Dijon Bourgogne, France.

Acknowledgments

Cytometry experiments were performed at the ImaFlow Facility, part of US58 BioSanD, INSERM, Université de Bourgogne Europe, Dijon, France. The authors thank Serge Monier for supplying the human umbilical vein endothelial cells and for his technical advice. Confocal microscopy images were obtained with the assistance of Chrystel DEULVOT, Plateforme DImaCell, AgroSup Dijon, Institut national de la recherche agronomique (INRA), University Bourgogne Franche-Comté, F-21000 Dijon, France. They also thank Victoria Bergas and Hélène Choubley from the DiviOmics Platform for expert technical assistance. The graphic abstract was created in BioRender (L. Mangin, 2025, https://BioRender.com/m87u859). All the authors have read and approved the final version of the manuscript. D. Leleu and D. Masson did the conceptualization. D. Leleu, C. Thomas, T. Gautier, and D. Masson carried out the methodology. D. Leleu, T. Pilot, L. Mangin, K. Van Dongen, and L. Proukhnitzky performed experiments. D. Leleu and D. Masson wrote the original draft. T. Pilot, K. Van Dongen, D. Denimal, T. Gautier, and C. Thomas reviewed and edited the article. M. Samson, A. Laubriet, E. Steinmetz, M. Rialland, L. Pierre, E. Groetz, and J.-P. Pais de Barros provided resources. D. Masson supervised the study.

Sources of Funding

This work was supported by French government grants managed by the French National Research Agency under the program "Investissements d'Avenir" with reference ANR-11-LABX-0021 (LipSTIC Labex) and "Targeting PUFA Metabolism in Macrophages in Cardiovascular Diseases" (PUMAs) with reference ANR-19-CE14-0020.

Disclosures

None.

Supplemental Material

Figures S1–S12
Major Resources Table

REFERENCES

1. Herrington W, Lacey B, Sherliker P, Armitage J, Lewington S. Epidemiology of atherosclerosis and the potential to reduce the global burden of atherothrombotic disease. *Circ Res*. 2016;118:535–546. doi: 10.1161/CIRCRESAHA.115.307611
2. Farahi L, Sinha SK, Lusis AJ. Roles of macrophages in atherogenesis. *Front Pharmacol*. 2021;12:785220. doi: 10.3389/fphar.2021.785220
3. Bobryshev YV, Ivanova EA, Chistiakov DA, Nikiforov NG, Orekhov AN. Macrophages and their role in atherosclerosis: pathophysiology and transcriptome analysis. *Biomed Res Int*. 2016;2016:9582430. doi: 10.1155/2016/9582430
4. Moore KJ, Sheedy FJ, Fisher EA. Macrophages in atherosclerosis: a dynamic balance. *Nat Rev Immunol*. 2013;13:709–721. doi: 10.1038/nri3520
5. Tabas I, Bornfeldt KE. Macrophage phenotype and function in different stages of atherosclerosis. *Circ Res*. 2016;118:653–667. doi: 10.1161/CIRCRESAHA.115.306256
6. Kim K, Shim D, Lee JS, Zaitsev K, Williams JW, Kim K-W, Jang M-Y, Seok Jang H, Yun TJ, Lee SH, et al. Transcriptome analysis reveals nonfoamy rather than foamy plaque macrophages are proinflammatory in atherosclerotic murine models. *Circ Res*. 2018;123:1127–1142. doi: 10.1161/CIRCRESAHA.118.312804
7. Cochain C, Vafadarnejad E, Arampatzi P, Pelisek J, Winkels H, Ley K, Wolf D, Saliba A-E, Zernecke A. Single-cell RNA-seq reveals the transcriptional landscape and heterogeneity of aortic macrophages in murine atherosclerosis. *Circ Res*. 2018;122:1661–1674. doi: 10.1161/CIRCRESAHA.117.312509
8. Zernecke A, Erhard F, Weinberger T, Schulz C, Ley K, Saliba A-E, Cochain C. Integrated single-cell analysis-based classification of vascular mononuclear phagocytes in mouse and human atherosclerosis. *Cardiovasc Res*. 2023;119:1676–1689. doi: 10.1093/cvr/cvac161
9. Dib L, Koneva LA, Edsfeldt A, Zurke Y-X, Sun J, Nitulescu M, Attar M, Lutgens E, Schmidt S, Lindholm MW, et al. Lipid-associated macrophages transition to an inflammatory state in human atherosclerosis, increasing the risk of cerebrovascular complications. *Nat Cardiovasc Res*. 2023;2:656–672. doi: 10.1038/s44161-023-00295-x
10. Slysz J, Sinha A, DeBerge M, Singh S, Avgousti H, Lee I, Glinton K, Nagasaka R, Dalal P, Alexandria S, et al. Single-cell profiling reveals inflammatory polarization of human carotid versus femoral plaque leukocytes. *JCI Insight*. 2023;8:e171359. doi: 10.1172/jci.insight.171359
11. Ravandi A, Babaei S, Leung R, Monge JC, Hoppe G, Hoff H, Kamido H, Kuksis A. Phospholipids and oxophospholipids in atherosclerotic plaques at different stages of plaque development. *Lipids*. 2004;39:97–109. doi: 10.1007/s11745-004-1207-5

12. Garcia-Cruset S, Carpenter KL, Guardiola F, Stein BK, Mitchinson MJ. Oxysterol profiles of normal human arteries, fatty streaks and advanced lesions. *Free Radic Res*. 2001;35:31–41. doi: 10.1080/10715760100300571
13. Carpenter KL, Taylor SE, van der Veen C, Williamson BK, Ballantine JA, Mitchinson MJ. Lipids and oxidised lipids in human atherosclerotic lesions at different stages of development. *Biochim Biophys Acta*. 1995;1256:141–150. doi: 10.1016/0005-2760(94)00247-v
14. Seimon TA, Nadolski MJ, Liao X, Magallon J, Nguyen M, Feric NT, Koschinsky ML, Harkewicz R, Witztum JL, Tsimikas S, et al. Atherogenic lipids and lipoproteins trigger CD36-TLR2-dependent apoptosis in macrophages undergoing endoplasmic reticulum stress. *Cell Metab*. 2010;12:467–482. doi: 10.1016/j.cmet.2010.09.010
15. Ricote M, Valledor AF, Glass CK. Decoding transcriptional programs regulated by PPARs and LXRs in the macrophage: effects on lipid homeostasis, inflammation, and atherosclerosis. *Arterioscler Thromb Vasc Biol*. 2004;24:230–239. doi: 10.1161/01.ATV.0000103951.67680.B1
16. Venkateswaran A, Laffitte BA, Joseph SB, Mak PA, Wilpitz DC, Edwards PA, Tontonoz P. Control of cellular cholesterol efflux by the nuclear oxysterol receptor LXRα. *Proc Natl Acad Sci USA*. 2000;97:12097–12102. doi: 10.1073/pnas.200367697
17. Thomas DG, Doran AC, Fotakis P, Westerterp M, Antonson P, Jiang H, Jiang X-C, Gustafsson J-A, Tabas I, Tall AR. LXR suppresses inflammatory gene expression and neutrophil migration through cis-repression and cholesterol efflux. *Cell Rep*. 2018;25:3774–3785.e4. doi: 10.1016/j.celrep.2018.11.100
18. Ito A, Hong C, Rong X, Zhu X, Tarling EJ, Hedde PN, Gratton E, Parks J, Tontonoz P. LXRs link metabolism to inflammation through Abca1-dependent regulation of membrane composition and TLR signaling. *eLife*. 2015;4:e08009. doi: 10.7554/eLife.08009
19. Ghisletti S, Huang W, Ogawa S, Pascual G, Lin M-E, Willson TM, Rosenfeld MG, Glass CK. Parallel SUMOylation-dependent pathways mediate gene- and signal-specific transrepression by LXRs and PPARgamma. *Mol Cell*. 2007;25:57–70. doi: 10.1016/j.molcel.2006.11.022
20. Ménégaut L, Thomas C, Jalil A, Julla JB, Magnani C, Ceroi A, Basmaciyan L, Dumont A, Le Goff W, Mathew MJ, et al. Interplay between liver X receptor and hypoxia inducible factor 1α potentiates interleukin-1β production in human macrophages. *Cell Rep*. 2020;31:107665. doi: 10.1016/j.celrep.2020.107665
21. González de la Aleja A, Herrero C, Torres-Torresano M, de la Rosa JV, Alonso B, Capa-Sardón E, Muller IB, Jansen G, Puig-Kröger A, Vega MA, et al. Activation of LXR nuclear receptors impairs the anti-inflammatory gene and functional profile of M-CSF-dependent human monocyte-derived macrophages. *Front Immunol*. 2022;13:835478. doi: 10.3389/fimmu.2022.835478
22. Sohrabi Y, Sonntag GVH, Braun LC, Lagache SMM, Liebmann M, Klotz L, Godfrey R, Kahles F, Waltenberger J, Findeisen HM. LXR activation induces a proinflammatory trained innate immunity-phenotype in human monocytes. *Front Immunol*. 2020;11:353. doi: 10.3389/fimmu.2020.00353
23. Tabraue C, Lara PC, De Mirecki-Garrido M, De La Rosa JV, López-Blanco F, Fernández-Pérez L, Boscá L, Castrillo A. LXR Signaling regulates macrophage survival and inflammation in response to ionizing radiation. *Int J Radiat Oncol Biol Phys*. 2019;104:913–923. doi: 10.1016/j.ijrobp.2019.03.028
24. Griffett K, Burris TP. Development of LXR inverse agonists to treat MAFLD, NASH, and other metabolic diseases. *Frontiers in medicine*. 2023;10:1102469. doi: 10.3389/fmed.2023.1102469
25. Zuercher WJ, Buckholz RG, Campobasso N, Collins JL, Galardi CM, Gampe RT, Hyatt SM, Merrihew SL, Moore JT, Oplinger JA, et al. Discovery of tertiary sulfonamides as potent liver X receptor antagonists. *J Med Chem*. 2010;53:3412–3416. doi: 10.1021/jm901797p
26. Toporova L, Grimaldi M, Boulahtouf A, Balaguer P. Assessing the selectivity of FXR, LXRs, CAR, and RORγ pharmaceutical ligands with reporter cell lines. *Front Pharmacol*. 2020;11:1122. doi: 10.3389/fphar.2020.01122
27. Griffett K, Solt LA, El-Gendy BEDM, Kamenecka TM, Burris TP. A liver-selective LXR inverse agonist that suppresses hepatic steatosis. *ACS Chem Biol*. 2013;8:559–567. doi: 10.1021/cb300541g
28. Wilhelm LP, Wendling C, Védie B, Kobayashi T, Chenard M-P, Tomasetto C, Drin G, Alpy F. STARD3 mediates endoplasmic reticulum-to-endosome cholesterol transport at membrane contact sites. *EMBO J*. 2017;36:1412–1433. doi: 10.15252/embj.201695917
29. Bolger AM, Lohse M, Usadel B. Trimmomatic: a flexible trimmer for Illumina sequence data. *Bioinformatics* 2014;30:2114–2120. doi: 10.1093/bioinformatics/btu170
30. Ishibashi M, Filomenko R, Rébé C, Chevriaux A, Varin A, Derangère V, Bessède G, Gambert P, Lagrost L, Masson D. Knock-down of the oxysterol receptor LXRα impairs cholesterol efflux in human primary macrophages: lack of compensation by LXRβ activation. *Biochem Pharmacol*. 2013;86:122–129. doi: 10.1016/j.bcp.2012.12.024
31. Yvan-Charvet L, Welch C, Pagler TA, Ranalletta M, Lamkanfi M, Han S, Ishibashi M, Li R, Wang N, Tall AR. Increased inflammatory gene expression in ABC transporter deficient macrophages: free cholesterol accumulation, increased signaling via toll-like receptors and neutrophil infiltration of atherosclerotic lesions. *Circulation*. 2008;118:1837–1847. doi: 10.1161/CIRCULATIONAHA.108.793869
32. Iwasaki Y, Suganami T, Hachiya R, Shirakawa I, Kim-Saijo M, Tanaka M, Hamaguchi M, Takai-Igarashi T, Nakai M, Miyamoto Y, et al. Activating transcription factor 4 links metabolic stress to interleukin-6 expression in macrophages. *Diabetes*. 2013;63:152–161. doi: 10.2337/db13-0757
33. Leitman DC, Ribeiro RC, Mackow ER, Baxter JD, West BL. Identification of a tumor necrosis factor-responsive element in the tumor necrosis factor alpha gene. *J Biol Chem*. 1991;266:9343–9346. doi: https://doi.org/10.1016/S0021-9258(18)92822-X
34. Falvo JV, Tsytsykova AV, Goldfeld AE. Transcriptional control of the TNF gene. *Curr Dir Autoimmun*. 2010;11:27–60. doi: 10.1159/000289196
35. Zhang W, Petrovic JM, Callaghan D, Jones A, Cui H, Howlett C, Stanimirovic D. Evidence that hypoxia-inducible factor-1 (HIF-1) mediates transcriptional activation of interleukin-1beta (IL-1beta) in astrocyte cultures. *J Neuroimmunol*. 2006;174:63–73. doi: 10.1016/j.jneuroim.2006.01.014
36. Hiscott J, Marois J, Garoufalis J, D'Addario M, Roulston A, Kwan I, Pepin N, Lacoste J, Nguyen H, Bensi G. Characterization of a functional NF-kappa B site in the human interleukin 1 beta promoter: evidence for a positive autoregulatory loop. *Mol Cell Biol*. 1993;13:6231–6240. doi: 10.1128/mcb.13.10.6231-6240.1993
37. Chistiakov DA, Bobryshev YV, Orekhov AN. Macrophage-mediated cholesterol handling in atherosclerosis. *J Cell Mol Med*. 2016;20:17–28. doi: 10.1111/jcmm.12689
38. Ekman S, Peter Slotte J. Effects of substrate composition on the esterification and hydrolysis activity of lysosomal acid sterol ester hydrolase. *Chem Phys Lipids*. 1987;45:13–25. doi: 10.1016/0009-3084(87)90036-3
39. Koivuniemi A, Heikelä M, Kovanen PT, Vattulainen I, Hyvönen MT. Atomistic simulations of phosphatidylcholines and cholesteryl esters in high-density lipoprotein-sized lipid droplet and trilayer: clues to cholesteryl ester transport and storage. *Biophys J*. 2009;96:4099–4108. doi: 10.1016/j.bpj.2009.01.058
40. Gonen A, Miller YI. From inert storage to biological activity-in search of identity for oxidized cholesteryl esters. *Front Endocrinol*. 2020;11:602252. doi: 10.3389/fendo.2020.602252
41. Hutchins PM, Murphy RC. Cholesteryl ester acyl oxidation and remodeling in murine macrophages: formation of oxidized phosphatidylcholine. *J Lipid Res*. 2012;53:1588–1597. doi: 10.1194/jlr.M026799
42. Brown MS, Goldstein JL, Krieger M, Ho YK, Anderson RG. Reversible accumulation of cholesteryl esters in macrophages incubated with acetylated lipoproteins. *J Cell Biol*. 1979;82:597–613. doi: 10.1083/jcb.82.3.597
43. Terasaka N, Wang N, Yvan-Charvet L, Tall AR. High-density lipoprotein protects macrophages from oxidized low-density lipoprotein-induced apoptosis by promoting efflux of 7-ketocholesterol via ABCG1. *Proc Natl Acad Sci USA*. 2007;104:15093–15098. doi: 10.1073/pnas.0704602104
44. Ménégaut L, Jalil A, Pilot T, van Dongen K, Crespy V, Steinmetz E, Pais de Barros JP, Geissler A, Le Goff W, Venteclef N, et al. Regulation of glycolytic genes in human macrophages by oxysterols: a potential role for liver X receptors. *Br J Pharmacol*. 2021;178:3124–3139. doi: 10.1111/bph.15358
45. Lemaire-Ewing S, Prunet C, Montange T, Vejux A, Berthier A, Bessède G, Corcos L, Gambert P, Néel D, Lizard G. Comparison of the cytotoxic, pro-oxidant and pro-inflammatory characteristics of different oxysterols. *Cell Biol Toxicol*. 2005;21:97–114. doi: 10.1007/s10565-005-0141-2
46. Larsson DA, Baird S, Nyhalah JD, Yuan XM, Li W. Oxysterol mixtures, in atheroma-relevant proportions, display synergistic and pro-apoptotic effects. *Free Radic Biol Med*. 2006;41:902–910. doi: 10.1016/j.freeradbiomed.2006.05.032
47. Canfrán-Duque A, Rotllan N, Zhang X, Andrés-Blasco I, Thompson BM, Sun J, Price NL, Fernández-Fuertes M, Fowler JW, Gómez-Coronado D, et al. Macrophage-derived 25-hydroxycholesterol promotes vascular inflammation, atherogenesis, and lesion remodeling. *Circulation*. 2023;147:388–408. doi: 10.1161/CIRCULATIONAHA.122.059062
48. Ou ZJ, Chen J, Dai WP, Liu X, Yang Y-K, Li Y, Lin Z-B, Wang T-T, Wu Y-Y, Su D-H, et al. 25-hydroxycholesterol impairs endothelial function and vasodilation by uncoupling and inhibiting endothelial nitric oxide synthase. *Am J Physiol Endocrinol Metab*. 2016;311:E781–E790. doi: 10.1152/ajpendo.00218.2016
49. Apostolakis S, Amanatidou V, Spandidos DA. Therapeutic implications of chemokine-mediated pathways in atherosclerosis: realistic

perspectives and utopias. *Acta Pharmacol Sin*. 2010;31:1103–1110. doi: 10.1038/aps.2010.131
50. Fatkhullina AR, Peshkova IO, Koltsova EK. The role of cytokines in the development of atherosclerosis. *Biochem Biokhimiia*. 2016;81:1358–1370. doi: 10.1134/S0006297916110134
51. Kleemann R, Zadelaar S, Kooistra T. Cytokines and atherosclerosis: a comprehensive review of studies in mice. *Cardiovasc Res*. 2008;79:360–376. doi: 10.1093/cvr/cvn120
52. Mallat Z, Besnard S, Duriez M, Deleuze V, Emmanuel F, Bureau MF, Soubrier F, Esposito B, Duez H, Fievet C, et al. Protective role of interleukin-10 in atherosclerosis. *Circ Res*. 1999;85:e17–e24. doi: 10.1161/01.res.85.8.e17
53. Simonini A, Moscucci M, Muller DWM, Bates ER, Pagani FD, Burdick MD, Strieter RM. IL-8 is an angiogenic factor in human coronary atherectomy tissue. *Circulation*. 2000;101:1519–1526. doi: 10.1161/01.cir.101.13.1519
54. Braunersreuther V, Mach F, Steffens S. The specific role of chemokines in atherosclerosis. *Thromb Haemost*. 2017;97:714–721. doi: 10.1160/th07-01-0036
55. Wang X, Wang L, Wen X, Zhang L, Jiang X, He G. Interleukin-18 and IL-18BP in inflammatory dermatological diseases. *Front Immunol*. 2023;14:955369. doi: 10.3389/fimmu.2023.955369
56. Pourcet B, Gage MC, León TE, Waddington KE, Pello OM, Steffensen KR, Castrillo A, Valledor AF, Pineda-Torra I. The nuclear receptor LXR modulates interleukin-18 levels in macrophages through multiple mechanisms. *Sci Rep*. 2016;6:25481. doi: 10.1038/srep25481
57. Keller AA, Maeß MB, Schnoor M, Scheiding B, Lorkowski S. Transfecting macrophages. *Methods Mol Biol*. 2018;1784:187–195. doi: 10.1007/978-1-4939-7837-3_18
58. Tannahill G, Curtis A, Adamik J, et al. Succinate is a danger signal that induces IL-1β via HIF-1α. *Nature*. 2013;496:238–242. doi: 10.1038/nature11986
59. Davignon J, Ganz P. Role of endothelial dysfunction in atherosclerosis. *Circulation*. 2004;109:III.–II27. doi: 10.1161/01.CIR.0000131515.03336.f8
60. Gimbrone MA, García-Cardeña G. Endothelial cell dysfunction and the pathobiology of atherosclerosis. *Circ Res*. 2016;118:620–636. doi: 10.1161/CIRCRESAHA.115.306301
61. Susser LI, Rayner KJ. Through the layers: how macrophages drive atherosclerosis across the vessel wall. *J Clin Invest*. 2022;132:e157011. doi: 10.1172/JCI157011
62. Ren X, Manzanares LD, Piccolo EB, Urbanczyk JM, Sullivan DP, Yalom LK, Bui TM, Lantz C, Najem H, Dulai PS, et al. Macrophage-endothelial cell crosstalk orchestrates neutrophil recruitment in inflamed mucosa. *J Clin Invest*. 2023;133:e170733. doi: 10.1172/JCI170733
63. Mackay F, Loetscher H, Stueber D, Gehr G, Lesslauer W. Tumor necrosis factor alpha (TNF-alpha)-induced cell adhesion to human endothelial cells is under dominant control of one TNF receptor type, TNF-R55. *J Exp Med*. 1993;177:1277–1286. doi: 10.1084/jem.177.5.1277
64. Kang S, Kishimoto T. Interplay between interleukin-6 signaling and the vascular endothelium in cytokine storms. *Exp Mol Med*. 2021;53:1116–1123. doi: 10.1038/s12276-021-00649-0
65. Schumacher N, Meyer D, Mauermann A, von der Heyde J, Wolf J, Schwarz J, Knittler K, Murphy G, Michalek M, Garbers C, et al. Shedding of endogenous interleukin-6 receptor (IL-6R) is governed by a disintegrin and metalloproteinase (ADAM) proteases while a full-length IL-6R isoform localizes to circulating microvesicles. *J Biol Chem*. 2015;290:26059–26071. doi: 10.1074/jbc.M115.649509
66. Deckert V, Perségol L, Viens L, Lizard G, Athias A, Lallemant C, Gambert P, Lagrost L. Inhibitors of arterial relaxation among components of human oxidized low-density lipoproteins. Cholesterol derivatives oxidized in position 7 are potent inhibitors of endothelium-dependent relaxation. *Circulation*. 1997;95:723–731. doi: 10.1161/01.cir.95.3.723
67. Yu L, Xu L, Chu H, Peng J, Sacharidou A, Hsieh H-H, Weinstock A, Khan S, Ma L, Durán JGB, et al. Macrophage-to-endothelial cell crosstalk by the cholesterol metabolite 27HC promotes atherosclerosis in male mice. *Nat Commun*. 2023;14:4101. doi: 10.1038/s41467-023-39586-z
68. Stannard AK, Riddell DR, Sacre SM, Tagalakis AD, Langer C, von Eckardstein A, Cullen P, Athanasopoulos T, Dickson G, Owen JS. Cell-derived apolipoprotein E (ApoE) particles inhibit vascular cell adhesion molecule-1 (VCAM-1) expression in human endothelial cells. *J Biol Chem*. 2001;276:46011–46016. doi: 10.1074/jbc.M104812200